Human Molecular Genetics, 2013, Vol. 22, No. 18 **3773–3788**
doi:10.1093/hmg/ddt228
Advance Access published on May 23, 2013

The giant spectrin βV couples the molecular motors to phototransduction and Usher syndrome type I proteins along their trafficking route

Samantha Papal[1,2,3], Matteo Cortese[1,2,3], Kirian Legendre[1,2,3], Nasrin Sorusch[6], Joseph Dragavon[4], Iman Sahly[1,2,3,5], Spencer Shorte[4], Uwe Wolfrum[6], Christine Petit[1,2,3,7] and Aziz El-Amraoui[1,2,3,*]

[1]Institut Pasteur, Unité de génétique et physiologie de l'audition, Paris F75015, France [2]Inserm UMRS1120, Paris, France [3]UPMC, Paris 6, France [4]Institut Pasteur, PFID-Imagopole, Paris, France [5]Institut de la vision, Syndrome de Usher et autres atteintes rétino-cochléaires, Paris, France [6]Institute of Zoology, Cell and Matrix Biology, Johannes Gutenberg University of Mainz, 55099 Mainz, Germany [7]Collège de France, Paris, France

Received April 2, 2013; Revised and Accepted May 16, 2013

Mutations in the myosin VIIa gene cause Usher syndrome type IB (USH1B), characterized by deaf-blindness. A delay of opsin trafficking has been observed in the retinal photoreceptor cells of myosin VIIa-deficient mice. We identified spectrin βV, the mammalian β-heavy spectrin, as a myosin VIIa- and rhodopsin-interacting partner in photoreceptor cells. Spectrin βV displays a polarized distribution from the Golgi apparatus to the base of the outer segment, which, unlike that of other β spectrins, matches the trafficking route of opsin and other phototransduction proteins. Formation of spectrin βV-rhodopsin complex could be detected in the differentiating photoreceptors as soon as their outer segment emerges. A failure of the spectrin βV-mediated coupling between myosin VIIa and opsin molecules thus probably accounts for the opsin transport delay in myosin VIIa-deficient mice. We showed that spectrin βV also associates with two USH1 proteins, sans (USH1G) and harmonin (USH1C). Spectrins are supposed to function as heteromers of α and β subunits, but fluorescence resonance energy transfer and *in vitro* binding experiments indicated that spectrin βV can also form homodimers, which likely supports its αII-independent βV functions. Finally, consistent with its distribution along the connecting cilia axonemes, spectrin βV binds to several subunits of the microtubule-based motor proteins, kinesin II and the dynein complex. We therefore suggest that spectrin βV homomers couple some USH1 proteins, opsin and other phototransduction proteins to both actin- and microtubule-based motors, thereby contributing to their transport towards the photoreceptor outer disks.

INTRODUCTION

Usher syndrome (USH) is the most frequent cause of inherited deaf-blindness in humans. Three clinical subtypes (USH1–3) have been defined according to the severity of the hearing impairment, the absence or presence of vestibular dysfunction, and the age of onset of retinitis pigmentosa that leads to blindness. USH1, the most severe clinical form, is characterized by congenital, severe to profound hearing loss, balance deficiency and early onset of retinitis pigmentosa before puberty (1–6). Six USH1 causal genes have been identified. They encode an actin-based motor, myosin VIIa (USH1B), a PDZ-domain-containing scaffold protein, harmonin (USH1C), two large cadherins, cadherin-23 (USH1D) and protocadherin-15 (USH1F), a scaffold protein with ankyrin repeats, sans (USH1G), and a calcium- and integrin-binding protein, CIB2 (USH1J) (3,6,7). Mutant mice lacking myosin VIIa, harmonin, cadherin-23, protocadherin-15 or sans display congenital profound deafness, faithfully mimicking the hearing impairment of USH1 patients (1,3). All five USH1 null mutant mice show a fragmentation of

*To whom correspondence should be addressed at: Unité de génétique et physiologie de l'audition, Inserm UMRS1120, Département de Neuroscience, Institut Pasteur, 25 rue du Dr Roux, 75015 Paris, France. Tel: +33 145688892; Email: aziz.el-amraoui@pasteur.fr or elaz@pasteur.fr

the hair bundle (8), the mechano-receptive structure by which auditory hair cells convert sound-evoked mechanical stimuli into receptor membrane potentials. The hair bundle consists of a staircase-like array of F-actin-rich microvilli, the stereocilia, which crowns the apical surface of the hair cells. In both the developing and mature hair bundle, cadherin-23 and protocadherin-15 have been proposed to form the interstereocilia links, which are anchored to the stereocilia actin filaments through direct interactions with myosin VIIa, harmonin b and sans (8–12).

As regards the visual phenotype, USH1 patients develop a rod-cone dystrophy, with electroretinogram abnormalities already detectable in 2-year-old affected children (13–16). In contrast, no such electroretinogram anomalies or abnormal visual phenotypes have been observed in the corresponding USH1 mutant mice (17–23). Such a discrepancy between mouse and human phenotypes could be explained by the existence of a major difference between rodents and primates in the architecture of photoreceptor cells (24). In the apical region of these cells, two distinct compartments can be distinguished: the photosensitive outer segment, which contains stacks of hundreds of membrane disks dedicated to the phototransduction process, and the inner segment, which contains the biosynthesis machinery. We recently showed that in human and non-human primate photoreceptor cells, USH1 proteins are localized at the interface between the inner and outer segments junction, and they are associated with the calyceal processes. These are F-actin filled long microvilli that crown the apical region of the inner segment and surround the basal outer disks. In contrast, mouse photoreceptors do not have typical calyceal processes, and lack USH1 proteins in this region (24). Together, these data led us to suggest that USH1 proteins form an adhesion belt around the basolateral region of the photoreceptor outer segment in humans, and that defects in this structure probably cause the retinal degeneration in USH1 patients (24). Additional roles for USH1 and USH2 proteins in the photoreceptor cells and/or other retinal cell types have been proposed (25–30). Notably, retinal abnormalities have been reported in some USH1 mutant mice, even though they do not display a retinal degeneration (26–28,31,32). Detailed analysis of photoreceptor cells from myosin VIIa-deficient mice has revealed altered assembly kinetics of the outer segment disks, and an abnormal accumulation of rhodopsin in the connecting cilium, the unique route between the inner and outer segments (32). Similar, but more severe opsin transport deficiency has been observed in Kif3a-deficient mice, due to defects in kinesin II, the microtubule-based anterograde motor protein (33,34). It has then been suggested that, similar to the kinesin/dynein motors, the actin-based motor protein myosin VIIa also participates in opsin transport through the photoreceptor connecting cilium (32,35). Yet, the molecular mechanisms elucidating how these motor proteins pick up opsin containing vesicles to allow their transport, and how the distinct motor complexes, myosin VIIa and kinesin/dynein, co-operate in transport of cargos along actin- and/or microtubule-based tracks remain unclear. These questions extend to other proteins of the transduction machinery, and possibly also to USH1 protein.

To address these issues, we sought proteins interacting with the tail of myosin VIIa using the yeast two-hybrid technique and a retinal cDNA library. We report here the identification of the non-classical spectrin, spectrin βV, as a myosin VIIa binding partner. Spectrin βV also associates with rhodopsin as well as several other key phototransduction proteins. Moreover, spectrin βV also interacts with the microtubule-based motors kinesin and dynein, which is consistent with its polarized and specific distribution pattern in the photoreceptor cells. Together, our findings led us to propose that spectrin βV multimers bridge post-Golgi vesicles to the photoreceptor motor proteins, and participate to their transfer towards the outer segment. Whether this extends to some transport anomalies observed in USH1 mutant mice is also investigated.

RESULTS AND DISCUSSION

Spectrin βV, the mammalian non-classical spectrin β subunit interacts with myosin VIIa

To identify myosin VIIa-interacting proteins, we used the C-terminal MyTH4/FERM domain of the human myosin VIIa as a bait (amino acids 1752–2215, accession number NP_000251) to screen a human retina yeast two-hybrid cDNA library (Fig. 1A). Among the potential ligands identified, a 320 amino acid prey (encoded by two different clones) that corresponds to the C-terminal region of the human spectrin βV subunit, hereafter referred to as βV-R29CT (amino acids 3355–3674), was detected (Fig. 1A). Spectrins consist of two subunits, α and β, which are aligned side to side to form higher order oligomers. In mammals, two α-spectrin subunits αI and αII, four classical β-spectrin subunits βI, βII, βIII and βIV, and a non-classical β subunit, βV, have been reported (36,37). Similar to other classical β spectrins, spectrin βV (molecular mass 417 kDa, accession number AAF65317.1) displays three distinct regions (38): an N-terminal region (amino acids 1–255) with two calponin homology (CH) motifs, a large central region (amino acids 256–3482) composed of 30 spectrin repeat units (the 30th being partial), instead of the 17 repeats found in classical β spectrins and a C-terminal region (amino acids 3483–3674) containing the pleckstrin homology (PH) domain (Fig. 1A).

To assess the specificity of the yeast two-hybrid interaction, the spectrin prey βV-R29CT was expressed in the yeast strain AMR70, and the recombinant strain was mated with recombinant L40 strains producing either myosin VIIa-MyTH4/FERM (amino acids 1752–2215), myosin VIIa-MyTH4 (amino acids 1752–2006), merlin (FERM domain-containing protein; amino acids 1–591) or an unrelated control protein, lamin C (amino acids 1–572). The spectrin βV-R29CT fragment did bind to myosin VIIa-MyTH4/FERM, whereas no interaction was obtained with myosin VIIa-MyTH4, merlin and lamin C (Fig. 1B). Consistently, in transfected HeLa cells, the GFP-tagged myosin VIIa tail co-localized with different myc-tagged spectrin βV fragments, specifically, βV-R29 (amino acids 3317–3674) and βV-PH (amino acids 3531–3643) (Fig. 1C). This interaction was further supported by the recruitment of GFP-tagged myosin VIIa tail at cell–cell junctions of the polarized epithelial cells LLC-PK-CL4, in which a spectrin βV fragment artificially targeted to the plasma membrane, the hEcad/βV-R29 chimera composed of the five extracellular cadherin repeats and transmembrane domain of human E-cadherin (hEcad) fused to βV-R29, was produced by

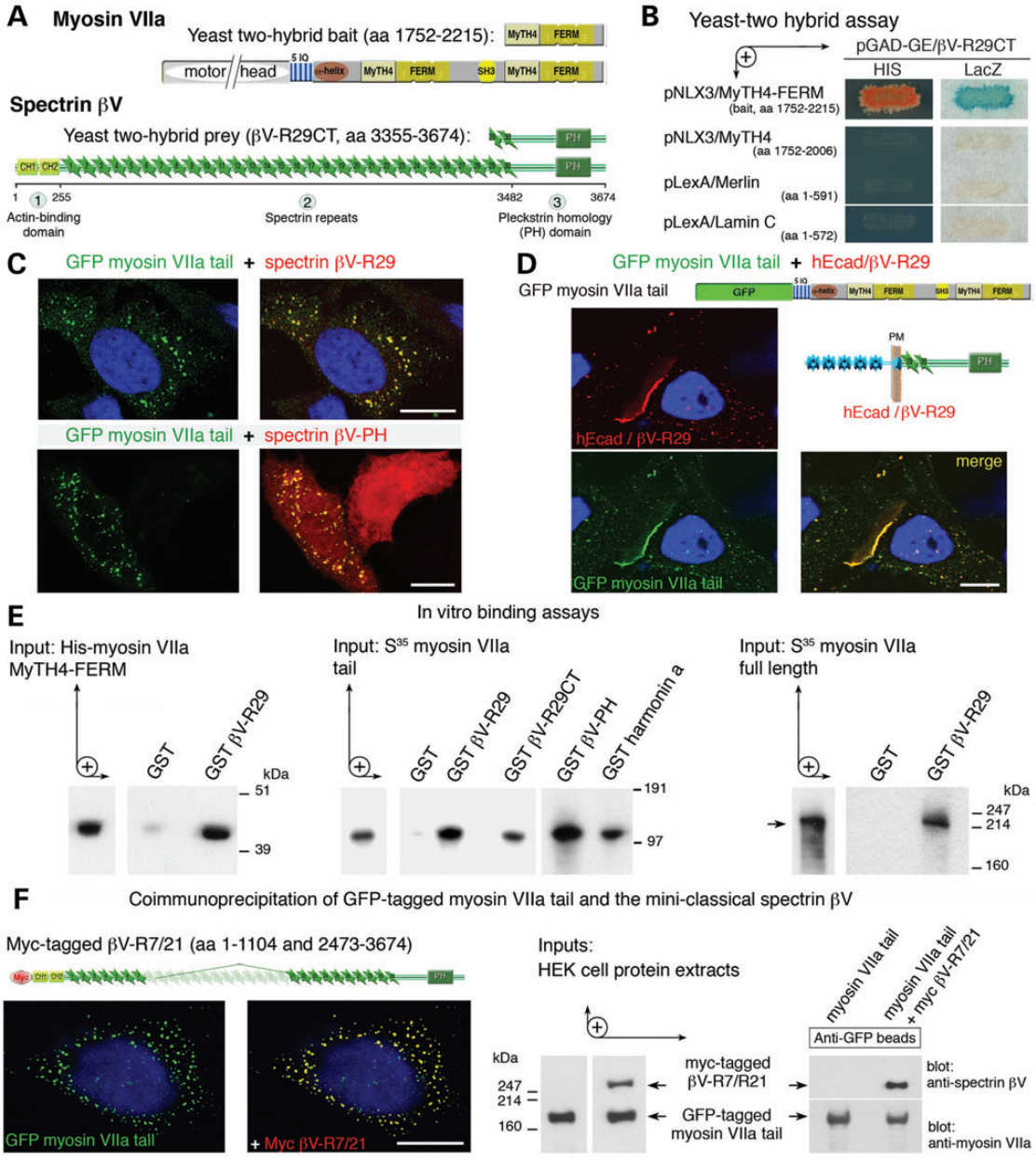

Figure 1. Spectrin βV directly interacts with myosin VIIa. (**A**) Predicted structures of the yeast two-hybrid (Y2H) myosin VIIa bait (MyTHY4-FERM) and spectrin βV prey. The Y2H prey corresponds to the C-terminal region of spectrin βV, which displays three regions: (i) the N-terminal two CH domains (amino acids 1–255), (ii) a long central region with 30 spectrin repeats (amino acids 256–3482), and (iii) a C-terminal region containing a PH domain (amino acids 3483–3674). (**B**) Yeast two-hybrid assay. Unlike the myosin VIIa bait (upper panel), the myosin VIIa-MyTH4 domain alone, the merlin FERM domain or the lamin C does not interact with spectrin βV-R29CT in yeast. (**C**) In co-transfected HeLa cells, GFP-tagged myosin VIIa tail (green) perfectly colocalizes throughout the cytoplasm with the myc-tagged spectrin βV-R29 and βV-PH (yellow). The presence of the myosin VIIa tail modifies the distribution pattern of βV-PH, i.e. the diffuse uniform distribution is changed into punctuated myosin VIIa and spectrin βV co-labelled structures, which further confirms the association between myosin VIIa and spectrin βV. (**D**) Also, when targeted to the cell–cell junction, using the hEcad/βV-R29 chimera, composed of the five extracellular cadherin repeats and transmembrane domain of human E-cadherin (hEcad) fused to the C-terminal region of spectrin, hEcad/βV-R29 is able to recruit the GFP-tagged myosin VIIa tail underneath the plasma membrane. (**E**) *In vitro* bindings. GST-tagged βV-R29, but not GST alone, binds to the purified His-tagged myosin VIIa-MyTH4/FERM fragment, the *in vitro* translated S^{35}-labelled myosin VIIa tail and the full-length protein. The GST-tagged βV-PH region is sufficient for spectrin βV-myosin VIIa interaction (middle panels). (**F**) Using HEK293 cells cotransfected with plasmids encoding GFP-tagged myosin VIIa tail and myc-tagged spectrin βV-R7/21, the two proteins specifically co-immunoprecipitated using anti-GFP conjugated coated beads. Bars = 10 μm.

cotransfected cells (Fig. 1D). The direct interaction between the two proteins was confirmed using direct *in vitro* binding assays. GST-tagged βV-R29 (amino acids 3317–3674), GST-tagged βV-PH and GST-harmonin a (the USH1C protein used as a positive control), but not GST alone, bound to His-myosin VIIa-MyTH4/FERM (amino acids 1752–2215), the myosin VIIa tail and also to the full-length myosin VIIa (Fig. 1E). Because myosin VIIa has been shown to interact with another PH-domain

containing protein, PHR1 (39), we tested whether it interacts with the PH domain of other β spectrins. We failed to observe an association between Flag βII-R13, the C-terminal fragment (amino acids 1595–2363) of spectrin βII, and the GFP-tagged myosin VIIa tail (Supplementary Material, Fig. S1D). Reciprocal experiments using biotin-tagged myosin VIIa truncated fusion proteins showed that the region containing the FERM domain (amino acids 1886–2215), but not the MyTH4 domain (amino acids 1731–1900), is required for the myosin VIIa interaction with βV-R29CT (see Supplementary Material, Fig. S2A). This interaction between spectrin and myosin VIIa is specific as no binding was observed between GST-tagged βV-R29 and several FERM-containing proteins, and myosins, specifically band 4.1, ezrin, merlin, the myosin X tail (amino acids 811–2062), the myosin XVa-MyTH4/FERM fragment (amino acids 2950–3511) or myosin IC (Supplementary Material, Fig. S2B). To test the interaction with a full-length spectrin βV, two human cDNA clones were obtained but, unfortunately, several errors and gaps were detected between the spectrin repeats 15 and 20 (see Supplementary Materials and Methods). To overcome this problem, we generated a mini-classical spectrin βV, referred to as βV-R7/21. This chimeric mini-spectrin βV lacks the spectrin repeats 8–20, but it displays the three regions found in classical spectrins, (i) the actin-binding domain, (ii) a central region with 17 spectrin repeats, and (iii) the C-terminal region containing the PH domain (Fig. 1F). Co-immunoprecipitation assays carried out on co-transfected HEK293 cells confirmed that the GFP-tagged myosin VIIa tail did immunoprecipitate with either myc-tagged βV-R7/21 (Fig. 1F) or βV-R29 (Supplementary Material, Fig. S1C).

Together, these data establish that spectrin βV specifically binds to myosin VIIa, an interaction that is mediated through their corresponding PH and FERM C-terminal domains, respectively.

Spectrin βV codistributes and interacts with myosin VIIa and rhodopsin in photoreceptor cells

To determine the cellular distribution of spectrin βV, we carried out confocal microscopy analyses on cryosections of adult cynomolgus monkey (*Macaca fascicularis*) and human retinas using affinity-purified antibodies produced against a human spectrin βV fragment (amino acids 3443–3668) (see Supplementary Materials and Methods). Spectrin βV immunostaining was detected in human and macaque photoreceptor cells, consistent with previous findings (38), and also in Müller glia cells (Fig. 2A). In contrast, unlike for myosin VIIa (40–42), no specific immunostaining for spectrin βV was detected in the retinal pigment epithelium cells, or in the synaptic region of photoreceptor cells (Fig. 2A, Supplementary Material, Fig. S3). In longitudinal sections, intense spectrin βV labelling was detected at the junction between the inner and outer segments, in both rod and cone photoreceptors (Fig. 2B–D). Given the presence of myosin VIIa and other USH1 proteins in the calyceal processes of photoreceptor cells, we asked whether spectrin βV is also present in these F-actin-based structures that are properly preserved only in perfused animals (24). We did not detect spectrin βV in the calyceal processes, which were visualized by their F-actin immunostaining that extends above the inner segment, and beyond the labelled connecting cilium (Fig. 2E).

Spectrin βV immunostaining was particularly abundant in the distal region of the inner segment, called the ellipsoid (Fig. 2B–D). Counterstaining with antibodies to rhodopsin, cone opsin and acetylated tubulin revealed that spectrin βV labelling also extended through the connecting cilium and along the associated axoneme alongside the opsin-labelled outer segment (Figs 2D and 3A). Consistently, applying pre- and post-embedding immuno-electron microscopy labelling in human and mouse retinas, we detected abundant spectrin βV labelling at the vicinity of microtubules spanning the connecting cilium and its axoneme (Fig. 3B), and in the region of newly formed disk membranes at the basal part of the outer segment (Supplementary Material, Fig. S4A and B). The post-embedding immunogold labelling also revealed decoration alongside the microtubules of the entire length of the connecting cilium (Supplementary Material, Fig. S4B).

Visual transduction occurs in the light sensing cilium organelle, the outer segment, which is continually renewed (43,44). In mammalian rods, new outer disks are produced at the base of outer segment every day and throughout lifetime (43). This outer disks turnover (∼10% every day) requires substantial vectorial transport of all disk components *de novo* synthesized in the inner segment (43,45–47). Every minute, ∼2000 rhodopsin molecules are transported towards the periciliary region and thus through the connecting cilium to the base of the outer segment, where new membranes are added at a rate of ∼77 cm^2/day (43–45,48). Of note, the distribution pattern of spectrin βV in the photoreceptor cells strictly matches the trafficking route of opsin molecules and the other components of the visual transduction cascade, i.e. arrestin, transducins, phosphodiesterase β and γ. This suggests that spectrin βV forms a guiding meshwork from the Golgi apparatus to the outer segment, supported by the absence of spectrin βV staining in the photoreceptor myoid and synaptic regions. Furthermore, by using retinal protein extracts from adult rat, we found that the anti-spectrin βV antibodies, but not the pre-immune serum or protein G alone (Fig. 3D), immunoprecipitated not only spectrin αII and band 4.1 protein (two natural ligands reported for all β spectrins), but also myosin VIIa and rhodopsin (Fig. 3D).

Together, our findings suggest that spectrin βV, located in the photoreceptor ellipsoid region, binds, *in vivo* and *in vitro*, to myosin VIIa and rhodopsin, two key proteins in photoreceptor cells functioning.

Spectrin βV can form homomers, and would thus display spectrin αII independent functions in the photoreceptor cells

Spectrins have so far been considered as heterotetrameric proteins of antiparallel α- and β-subunits (Fig. 4A), presenting two actin-binding domains at both ends of the tetramer, which enables them to crosslink actin filaments into branched networks (36,37,49,50). The identity of spectrin β subunit, its subcellular localization and also the spectrum of corresponding binding partners (including among other spectrins) thus probably guide the specificity of spectrins' function. By analysing the distribution patterns of αII spectrin and of the five spectrin β subunits in the retina, we found that, apart from βII and αII (Fig. 4B; see also 51,52), only a significant βV spectrin labelling could be detected in photoreceptor cells (Fig. 4B). In these cells, βV displayed a unique cytoplasmic immunostaining along the

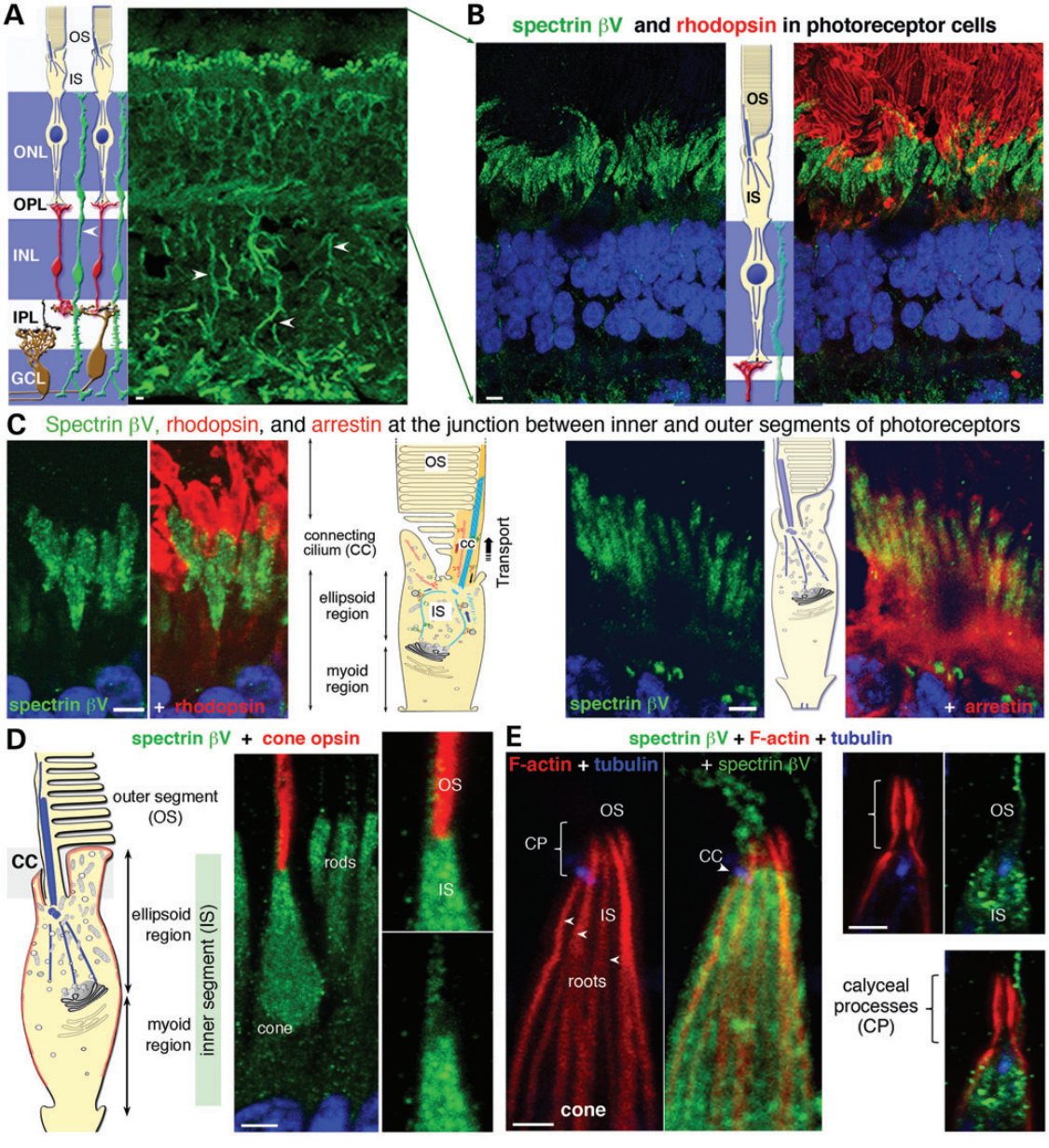

Figure 2. Polarized distribution of spectrin βV in the photoreceptor cells. (**A** and **B**) Longitudinal cross-sections of macaque (A) and human (B) retinas (non-perfused animals). The organization of the vertebrate neural retina is shown on the left. Prominent immunostaining for spectrin βV (green) is observed in the photoreceptor cells, and glial Muller cells (arrowheads in A) that spread throughout the neuroretina. In photoreceptor cells, spectrin βV is detected at the junction between the inner (IS) and outer (OS) segments. (**C** and **D**) In both cone and rod of dark-adapted photoreceptors, spectrin βV is particularly abundant below the opsin-labelled OS, in the distal region of the arrestin-labelled IS, called the ellipsoid. (**E**) Macaque retinas (perfused animals). A phalloidin-stained retina, illustrating the presence of the F-actin labelled calyceal processes (CP) and their roots (arrowheads) in the apical region of the inner segment of a cone photoreceptor cell. Note that spectrin βV immunolabelling is absent from the F-actin labelled calyceal processes, extending above the connecting cilium (blue). DAPI nuclear staining (blue) delineates the outer nuclear layer (ONL). OPL, outer plexiform layer; INL, inner nuclear layer; IPL, inner plexiform layer; GCL, ganglion cell layer. Bars = 10 μm.

trafficking route from the Golgi apparatus towards the base of the photoreceptor outer segment (Fig. 4B and C). This contrasted with the distribution pattern of αII and βII spectrin subunits, which were both observed along the plasma membrane of the inner segment (Fig. 4B and C), as previously reported (52,53). Spectrins αII/βII, similar to αII/βIII (54), have been shown to be involved in the sorting and transport of proteins to the lateral plasma membrane (52). Double labelling showed that spectrin βV immunostaining does not colocalize with spectrins βII and αII in the photoreceptor inner segment ellipsoid (Fig. 4C) or along outer segment axoneme (Fig. 4D), which qualifies spectrin βV as the spectrin being involved in targeting towards the apical membrane, the outer segment.

So far, little attention has been paid to whether there exists mixed or strict co-distribution of spectrin α and β subunits in a given cell type. The distinct spectrin distribution patterns we show here in photoreceptor cells raises the attractive possibility that, at least in some compartments, the spectrin subunits αII and

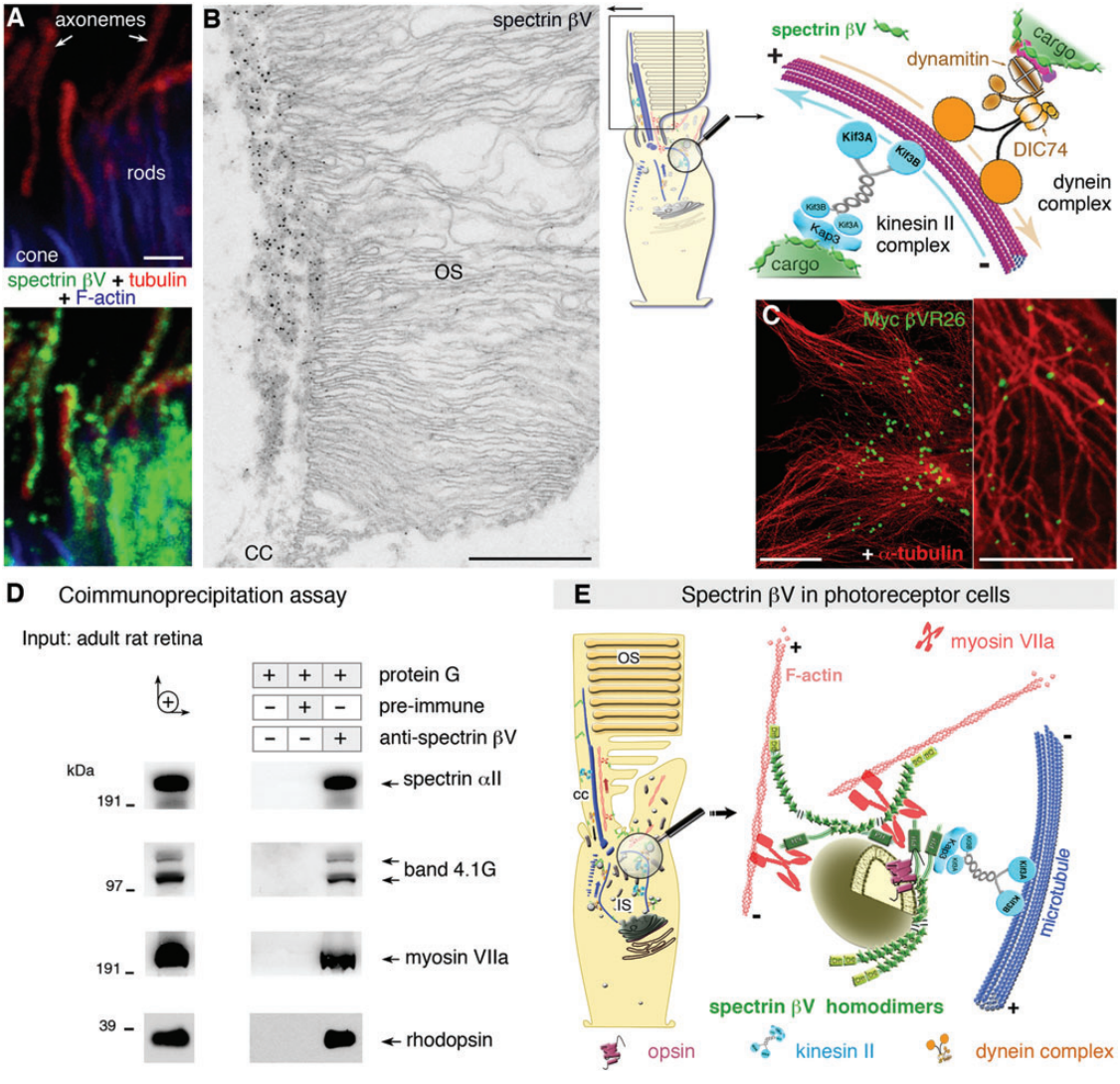

Figure 3. Spectrin βV and microtubules in the photoreceptor cells. (**A** and **B**) Macaque (A) and human (B) retinas. A spectrin βV labelling is also detected in the connecting cilium, and extends also along the axoneme bordering the outer disks (A and B). Consistently, spectrin βV is detected in the axonemal cytoplasm of the outer segment of a human rod photoreceptor by pre-embedding immunoelectron microscopy (B). The right upper panel in (B) is a schematic representation of the kinesin II and dynein motor complexes, involved in anterograde and retrograde transport along microtubules, respectively. (**C**) In transfected HeLa cells producing the myc-tagged βV-R26, the spectrin fusion protein (green) displays cytoplamsic puncta that are aligned along microtubules (red). (**D**) Spectrin βV forms *in vivo* complexes with myosin VIIa and rhodopsin. Using adult rat retinal lysates, the anti-spectrin βV antibody, but not the corresponding pre-immune serum or protein G alone, immunoprecipitates both myosin VIIa and rhodopsin. The immunoprecipitation of spectrin αII and band 4.1 protein are shown as positive controls. (**E**) Schematic diagrams of the apical compartment of photoreceptor cells illustrating how spectrin βV homomers, in the absence of spectrin αII, could bring together membranes or membrane-associated proteins of intracellular organelles, allowing their transport towards and within the connecting cilium. Spectrin βV is also qualified to switch organelles between microfilament and microtubule tracks, thanks to its interaction with the actin- and microtubule-based motor proteins. The microfilament (F-actin) and microtubule cytoskeletons are indicated. Bars = 10 μm (A and C); 500 nm (B).

βV do function independently. For spectrin βV molecules to be able to cross-link actin filaments, one possibility is a self-association of the monomers through their C-terminal region. We used complementary approaches to investigate this possibility. In HeLa cotransfected cells, we observed that CFP-tagged βV-R23 strictly colocalized with myc-tagged βV-R26 (Fig. 5A), but not with Flag-tagged βII-R13 (Fig. 5B). To address a possible spectrin βV self-association in living cells, CFP-tagged βV-R23 (amino acids 2684–3674) and YFP-tagged βV-R29 (amino acids 3317–3674) were used as donor and acceptor, respectively. The interaction between the cyan and yellow fluorescent proteins was monitored by fluorescence resonance energy transfer (FRET) microscopy (Fig. 5C and D). Analysis was performed after transient expression in single (Fig. 5C, upper panels) and double-transfected (Fig. 5C, lower panels) cells. The lifetime decay of donor fluorescence is characteristic of FRET occurrence between the two fluorophores. Excitation was carried out at 445 nm, and FRET between the two fusion proteins was then monitored using fluorescence lifetime imaging microscopy. In HeLa cells producing either CFP-tagged βV-R23 or YFP-tagged βV-R29, the lifetime fluorescence of CFP and YFP was about 3.72 ns (orange in Fig. 5C) and 1.9 ns

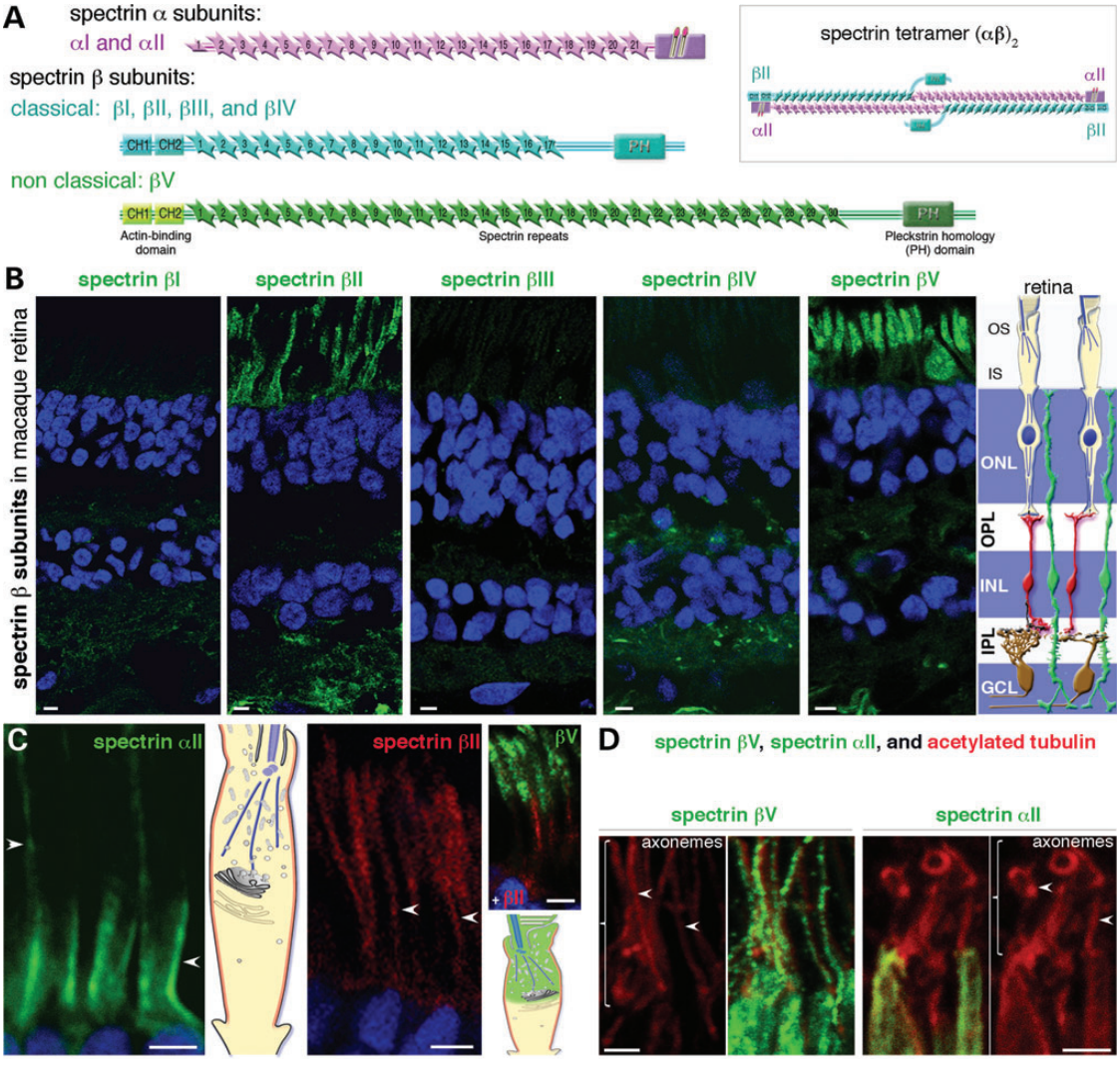

Figure 4. Distribution of different spectrins in the retina. (**A**) Spectrins consist of two subunits, α and β, that are aligned side to side to form heterodimers, which in turn can form higher oligomers (generally tetramers) by head-to-head interactions (see boxed area). In mammals, two spectrin α subunits αI and αII, four classical spectrin β subunits, βI, βII, βIII and βIV, and a non-classical β subunit, βV, have been reported. (**B**–**D**) Spectrin αII- and β-subunits in macaque retinas (non-perfused animals). The immunostainings for spectrins αII and βII are present in several cell types across the retinal layers, including photoreceptor cells where most of the labelling is detected along the inner segment plasma membrane (B and C). Under the same conditions, no significant labelling was obtained for spectrins βI and βIII in photoreceptor cells, while spectrin βIV-immunoreactive structures were observed in neuronal extensions (nodes of Ranvier) in the outer and inner plexiform layers (B). Spectrins βV and βII are distributed in different compartments of the photoreceptor cells (C). The only spectrin β immunostaining that is detected along the connecting cilium and its axoneme is that of spectrin βV (D). Bars = 10 μm (B); 5 μm (C), 2 μm (D).

(light blue in Fig. 5C), respectively, which are the expected values in the absence of FRET. The mean lifetime measurements from 10 cells are reported in Figure 5D. In contrast, in co-transfected cells producing both CFP-tagged βV-R23 and YFP-tagged βV-R29, we found a significant decrease in the donor (CFP-tagged βV-R23) lifetime (from 3.72 to 2.165 ns) (Fig. 5D). An increase in the lifetime fluorescence of the acceptor (YFP-tagged βV-R29, from 1.9 to 2.3 ns) was also observed (Fig. 5D). Together, our data establish a direct homodimeric interaction between the two spectrin βV fragments. Using *in vitro* binding experiments, we could show that the spectrin βV self-association did occur through the last C-terminal spectrin repeats (R29-R30) (Fig. 5E). We next tested if the spectrin βII subunit, which is present in photoreceptor cells, also can form heterotypic dimers with spectrin βV. No interaction was observed between spectrin βV and flag-tagged βII-R13 (Fig. 5B and F, and data not shown), excluding a mixed association between βV and βII spectrin subunits.

We next examined a possible effect of spectrin βV on cellular membrane compartments using transfected HeLa cells. Previous studies in Drosophila have shown that overexpression of the C-terminal region of β-heavy spectrin, the Drosophila ortholog of spectrin βV, affects cell shape and epithelial development, features ascribed to defects in membrane and protein trafficking (55,56). Comparative analyses were carried out in HeLa cells producing each of two myc-tagged spectrin βV fragments, βV-R7/21 (chimeric full-length mini-classical spectrin βV), βV-R26 (amino acids 3002–3674) or the flag-tagged spectrin

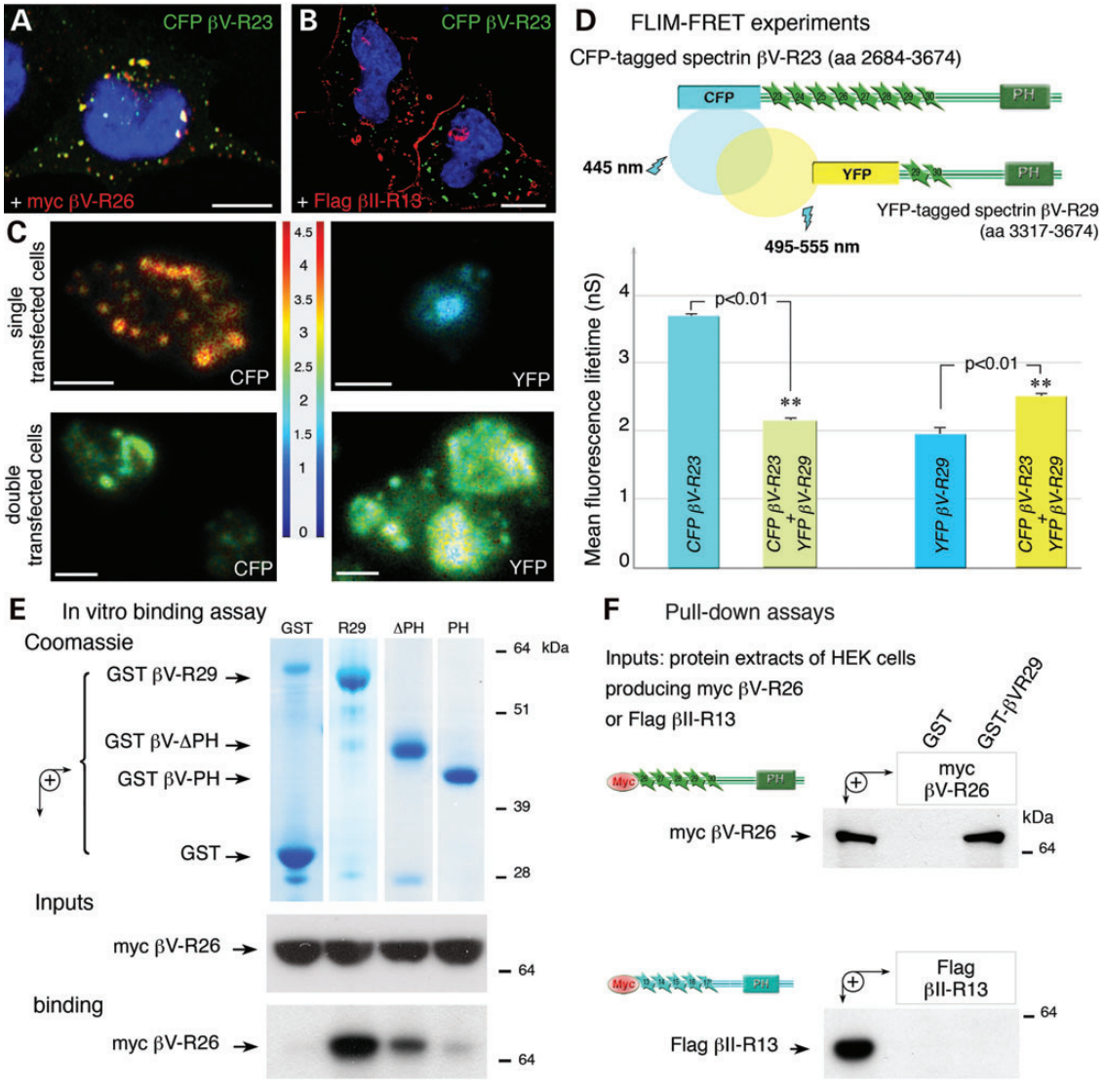

Figure 5. Spectrin βV forms homotypic homodimers. (**A** and **B**) In cotransfected HeLa cells, the CFP-tagged βV-R23 perfectly colocalized with myc-tagged βV-R26 (A), but not with the flag-tagged equivalent region in spectrin βII, βII-R13 (B). (**C**) Fluorescence lifetime images of representative cells, illustrating FRET efficiency in living cells transfected by CFP-tagged βV-R23 and YFP-tagged βV-R29 fusion proteins. A decrease in the donor (CFP-tagged βV-R23) lifetime (from 3.72 to 2.165 ns) is observed in transfected cells producing both CFP-tagged βV-R23 and YFP-tagged βV-R29, confirming the occurrence of FRET between the two fusion proteins. Low fluorescence lifetime is represented in blue, whereas high fluorescence lifetime is in red. (**D**) The schematic graphs represent the mean fluorescence lifetime (ns) of CFP and YFP fusion protein when they are alone, or when they interact with each other. The mean lifetime was calculated with the lifetime values extracted from three regions of interest on a minimum of 10 cells per experiment. The mean values obtained from several cells, and experiments are presented in (D). (**E**) Using different GST-tagged fusions, βV-R29, βV-ΔPH, βV-PH or GST alone, incubated with equal amounts of myc-tagged βV-R26, only GST-tagged βV-R29 and GST-tagged βV-ΔPH interact with myc-tagged βV-R26. (**F**) Pull-down assays. GST-tagged βV-R29 specifically binds to the myc-tagged spectrin βV-R26, but not the flag-tagged equivalent region in spectrin βII, βII-R13. Bars = 10 μm.

βII C-terminal fragment βII-R13 (amino acids 1595–2363) (Fig. 6). Analysis of transfected HeLa cells revealed two abnormal phenotypes specifically observed in βV-R26 producing cells (Fig. 6). The architecture of the Golgi apparatus was impaired in 40% of these transfected cells, as revealed by immunostaining the Golgi-matrix protein, GM130 (Fig. 6B). Instead of the compact and normal Golgi stacks observed in non-transfected cells, or in transfected cells producing myc-tagged βV-R7/21 (Fig. 6A) or flag-tagged βII-R13 (data not shown), the Golgi apparatus in βV-R26-producing cells was present as dispersed fragmented structures (Fig. 6B). Furthermore, the overexpression of myc-tagged βV-R26 was correlated with a reduction in the fluorescence of the lysosomal marker Lamp1, suggesting a disruption in lysosomal trafficking (Fig. 6C). We found that there was a 1.67-fold decrease in Lamp1 staining intensity in cells overexpressing βV-R26, compared with non-transfected cells ($P < 0.0001$) (Fig. 6D, and see Supplementary Materials and Methods). In contrast, we did not observe such a decrease in HeLa cells producing either the chimeric βV spectrin protein βV-R7/21 ($P = 0.8985$) or the flag-tagged βII-R13 ($P = 0.2034$) (Fig. 6E–H). Together, these data suggest that overexpression of the spectrin C-terminal region affects Golgi

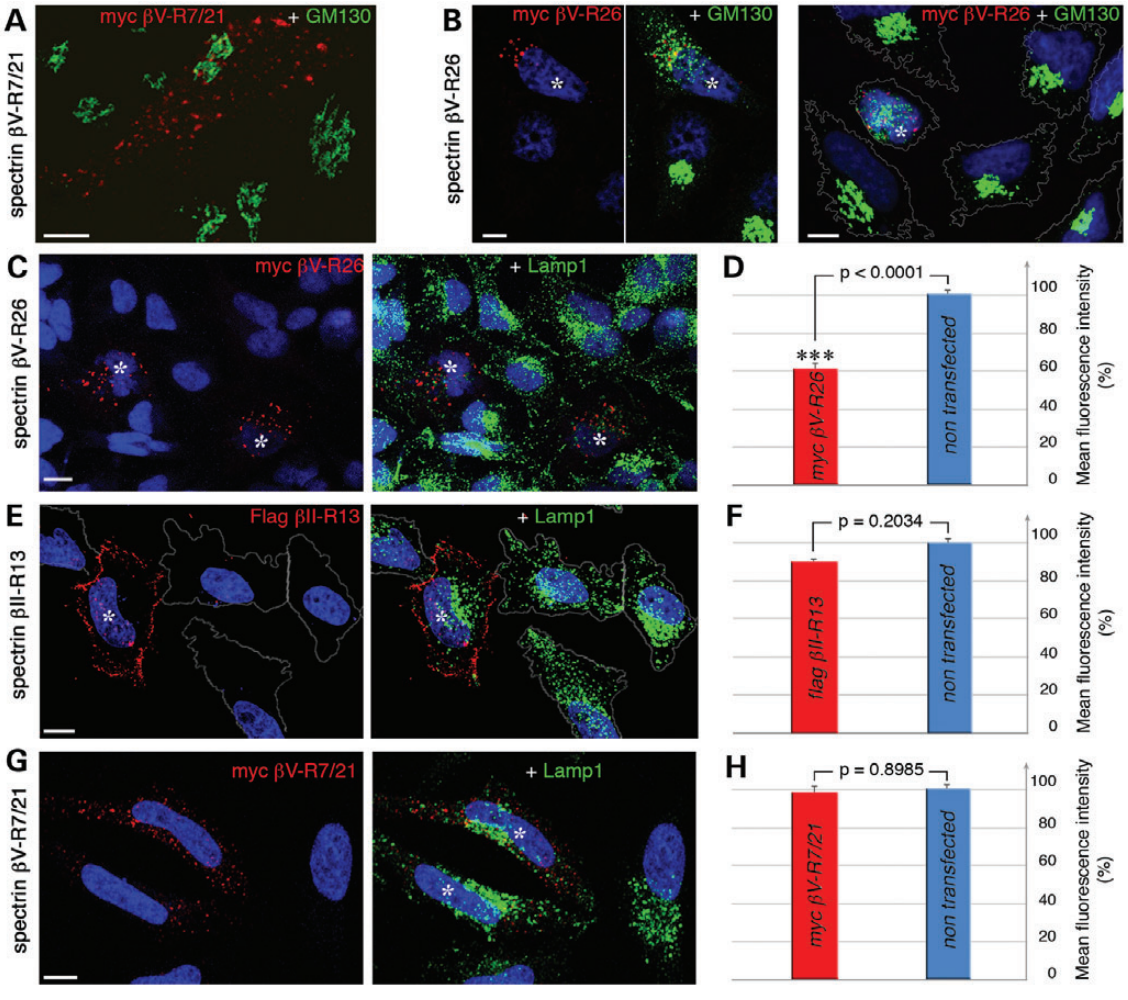

Figure 6. Overexpression of the spectrin βV C-terminal region affects Golgi apparatus architecture and interferes with lysosomal trafficking. (**A** and **B**) The architecture of the Golgi apparatus, visualized by GM130 immunostaining (green), is affected in transfected cells producing the C-terminal region of spectrin βV, βV-R26 (red in B), but not mini-classical spectrin βV-R7/21 (red in A). (**C**–**H**) Overexpression of βV-R26 also affects lysosomal compartment, visualized by Lamp1 immunostaining. Quantification of immunofluorescence in transfected cells producing spectrin βV-R26 (C and D), spectrin βII-R13 (E and F) or the mini-classical spectrin βV-R7/21 (G and H) was performed. The overexpression of βV-R26, but not βV-R7/21 or βII-R13, significantly reduces the extent of Lamp1 immunostaining (D). Bars = 10 μm.

apparatus structure and cellular membrane compartments (e.g. lysosomes).

Our findings provide evidence that spectrin βV can form homotypic homodimers, which, in the absence of spectrin α, enables βV subunits multimers to tether vesicular intracellular membranes allowing their connection to the adjacent cytoskeleton.

Spectrin βV associates with microtubule-based motors in the differentiating photoreceptor cells

In photoreceptor cells, protein transport does not rely on actin-based motors only. A bidirectional trafficking towards and along the connecting cilium occurs along microtubules, mediated by anterograde and retrograde movements of molecular motors (46,57,58). The cytoplasmic dynein complex conveys cargos from the Golgi apparatus towards the base of the connecting cilium (59–61), where the kinesin complex takes over to translocate ciliary membrane associated components towards the outer segment (Fig. 3A and B). Spectrin βV association with the connecting cilium and the outer segment axoneme (Fig. 3A), as well as the co-alignment of myc-tagged βVR29 puncta with microtubules in transfected HeLa cells (Fig. 3C), prompted us to seek for its possible link with microtubule-based motors. We first tested whether spectrin βV can associate with the dynein complex. Two subunits of this motor complex, dynein intermediate chain (DIC) and dynamitin (p50), but not centrin, a Ca^{2+}-binding protein of the connecting cilium (62,63) used as a control protein, were indeed co-immunoprecipitated by anti-spectrin βV antibodies (Fig. 7A). We also sought a possible association between spectrin βV and kinesin II, a heterotrimer consisting of two heavy chains, Kif3a and Kif3b, and an accessory subunit, Kap3 (kinesin-associated polypeptide 3) (Fig. 7A). We found that Kif3a subunit coimmunoprecipitated with spectrin βV using the anti-spectrin βV antibody (Fig. 7A). The interaction between spectrin βV and Kif3a does not depend on kinesin-microtubule interactions, as GST-tagged βV-R29 binding to Kif3a was insensitive to ATP- and remained

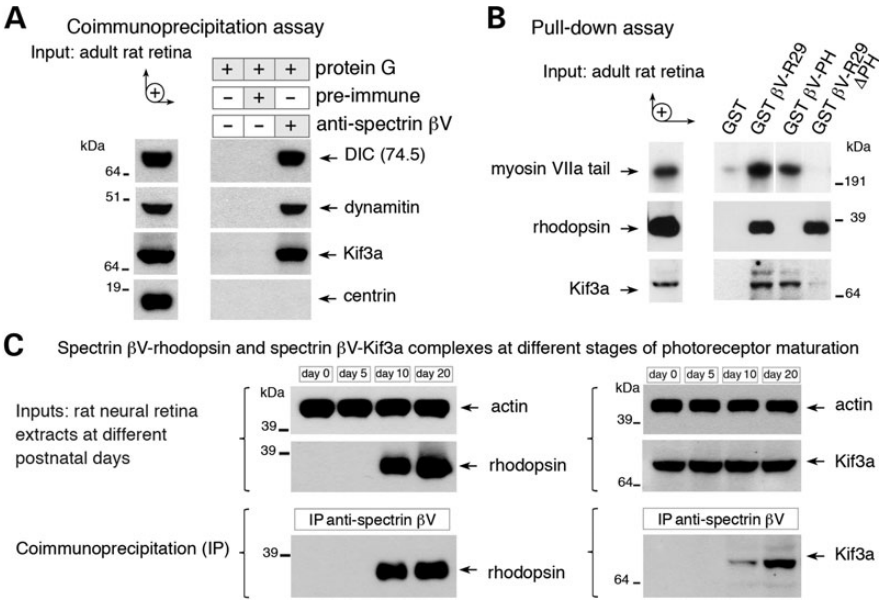

Figure 7. Spectrin βV and motor proteins in the differentiating photoreceptor cells. (**A**) Spectrin βV and microtubule-base motor complexes. The anti-spectrin βV antibody immunoprecipitates the dynein light intermediate chain (DIC70), dynamitin/p50, the kinesin II subunit, Kif3A, but not centrin, a component of the connecting cilium. (**B**) Mapping of the myosin VIIa-, Kif3a- and rhodopsin-binding region on spectrin βV. GST-tagged βV-R29, GST-tagged βV-R29ΔPH, GST-tagged βV-PH and GST alone were incubated with total protein extracts of P35 rat retinas. GST-tagged βV-PH binds to both myosin VIIa, and Kif3a, while GST-tagged βV-R29ΔPH interacts with rhodopsin. (**C**) Rhodopsin–spectrin βV-motor complex reflects the progressive formation and maturation of retinal photoreceptor cells. The same amounts of proteins (blot with anti-actin) were used at each developmental stage, at P0 and P5 (stages at which the outer disks are not yet differentiated), P10 and P20 (differentiating and mature stage). The specific association between spectrin βV-rhodopsin and spectrin βV-Kif3a take place only from P10 onwards, which coincides with the opsin expression and is after the emergence of the outer segment. Molecular mass is indicated in kilodaltons (kDa).

stable at high salt (<450 mM) concentrations (Supplementary Material, Fig. S5A and B). Interestingly, immunoprecipitations carried out at different stages of murine photoreceptor maturation (see Supplementary Material, Fig. S3C) showed that the formation of the spectrin βV-opsin and spectrin βV-microtubule associated motor complexes parallels the emergence of the outer segments in the photoreceptor cells (Fig. 7C). Anti-spectrin βV antibodies incubated with retinal protein extracts derived from rats at P0 (retina with immature photoreceptors), P5 (photoreceptor cells just starting to develop their connecting cilia), P10 (photoreceptor cells have developed outer disks) or P20 (mature retina) detected spectrin βV-opsin and spectrin βV-Kif3a complexes from P10 onwards (Fig. 7C), when the synthesis of opsin molecules had increased and the photoreceptor outer disks start to form (64,65).

To address whether spectrin βV can interact simultaneously with cargos and the different molecular motors, we examined whether the same or distinct domains of spectrin βV C-terminal region are involved in myosin VIIa-, kinesin II- and rhodopsin-bindings (Fig. 7B). We found that GST-tagged βV-PH was sufficient to interact with either myosin VIIa or Kif3a, whereas GST-tagged βV-R29ΔPH bound only to rhodopsin (Fig. 7B). Therefore, a spectrin βV monomer can bind simultaneously to both rhodopsin and a motor protein, either myosin VIIa or kinesin II. These motors are likely to compete for their interaction with the PH domain of spectrin βV. Nonetheless, thanks to its homomerization, spectrin βV multimers (almost twice as long as the classical spectrins) tethered to opsin may still bind, either independently or concomitantly, to distinct cytoskeleton-associated motors, thereby allowing the possibility of cargos-switching between actin filaments and microtubule tracks.

Spectrin βV bridges phototransduction and USH1 proteins to cargos in the photoreceptor cells

In photoreceptor cells, arrestin and transducin have been shown to undergo light-driven reversible translocation between the inner and outer segments, a process that has been shown to require an intact cytoskeleton (66). Recently, defects in the translocation of these proteins have been reported when myosin VIIa-deficient mice are exposed to light at 2500 Lux illumination (67). Notably, a delayed transducin translocation has been reported in these mice, which infers that myosin VIIa might contribute also to light-dependent bidirectional movement of molecules across the connecting cilium (67). Based on the results showing spectrin βV interaction with myosin VIIa and rhodopsin (Figs 1 and 3), we explored the possibility that spectrin βV associates also with arrestin and transducin, and extended our investigation to some other proteins involved in the phototransduction machinery (Fig. 8A, left panel). Pull-down and co-immunoprecipitation experiments, using P35 rat retinal protein lysates, showed that spectrin βV associates, both *in vitro* (Supplementary Material, Fig. S5C) and *in vivo* (Fig. 8A, right panels), with transducins β1 (rod transducin) and β3 (cone transducin, see Supplementary Material, Fig. S5C), arrestin, and PDE6γ, a prenyl-binding protein involved in the solubilization of phosphodiesterase from the rod outer segment disc membrane during phototransduction (Fig. 8A, right panels).

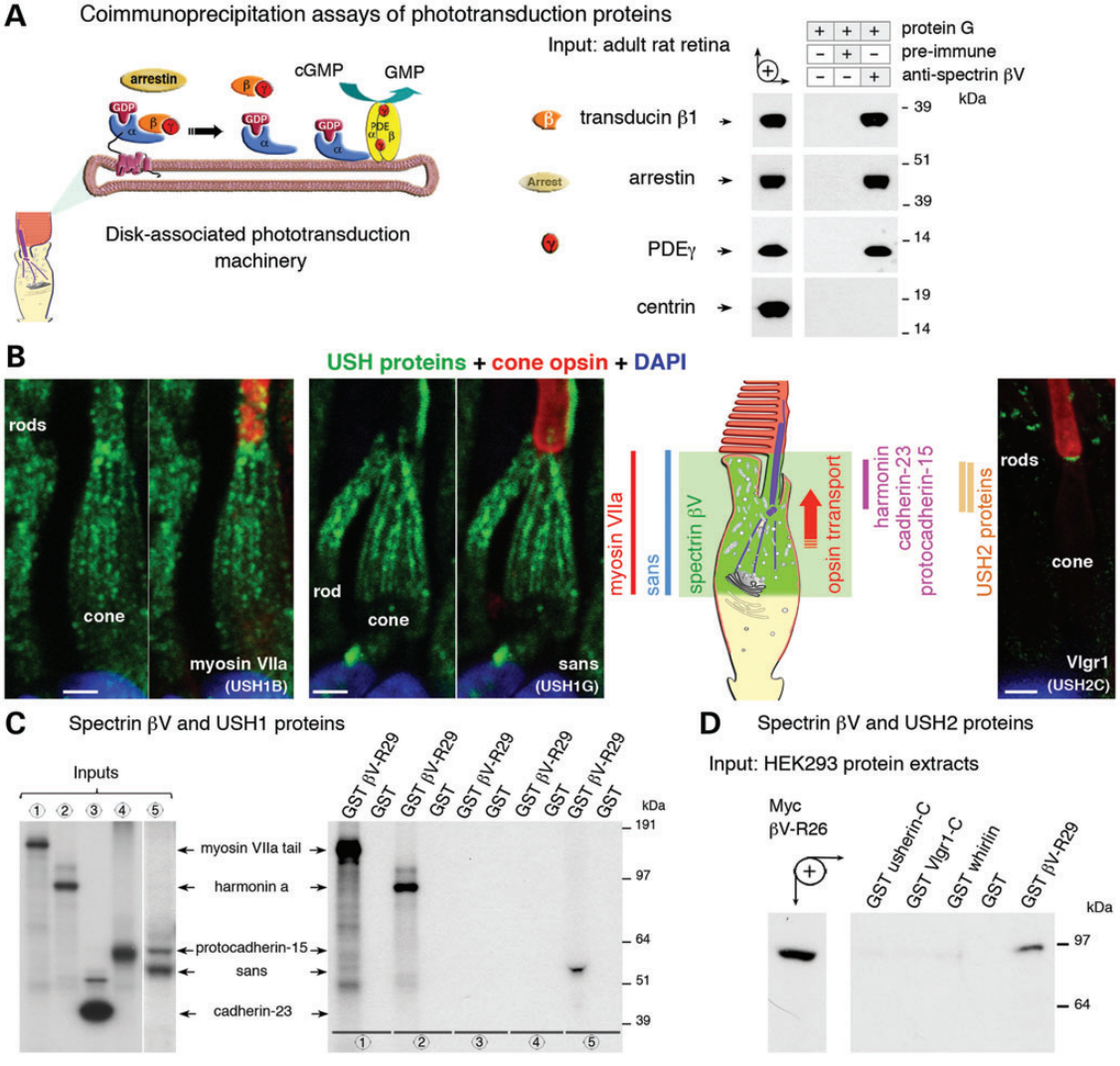

Figure 8. Spectrin βV is a member of the USH1 protein network. (**A**) Spectrin βV associates with key proteins of the photoreceptor outer segment. The association of several key proteins of the phototranduction machinery (left panel) with spectrin βV was tested. Transducin β1, arrestin and PDEγ co-immunoprecipitate with spectrin βV (right panels). Under these conditions, anti-spectrin βV immunoprecipitates do not contain the connecting cilium component centrin. (**B**) Longitudinal sections of macaque retinas. The distribution patterns of the USH1 proteins myosin VIIa, and sans (left panels), overlap with that of spectrin βV, in the ellipsoid region of photoreceptor cells. Spectrin βV also is present around the periciliary ridge region, a collar region around and alongside the connecting cilium, where the docking of membranes and proteins, en route to the outer segment, occurs, and where USH2 proteins, including Vlgr1 (right panel), are detected (B). (**C** and **D**) Interactions between spectrin βV and USH proteins. GST-tagged βV-R29 interacts with myc-tagged sans and GFP-tagged harmonin (isoform a), and GFP-tagged myosin VIIa tail (used as a positive control). No binding is observed with myc-tagged cytoplasmic regions of protocadherin-15 and cadherin-23 (C). In the reciprocal experiments, unlike GST-tagged βV-R29 (used as a positive control), none of the GST-tagged USH2 proteins, usherin-cytodomain, Vlgr1-cytodomain and whirlin, interacts with myc-tagged βV-R26 (D).

Considering that the spectrin βV distribution pattern in the ellipsoid region of the photoreceptor cells overlaps with that of USH1 (inner segment and/or connecting cilium) and USH2 proteins (periciliary region) (Fig. 8B, see also 24,29,30,35,41), we investigated whether spectrin βV may interact also with other USH1 proteins. GST-tagged βV-R29 or GST alone were incubated with protein extracts of HEK293 cells producing either the GFP-tagged myosin VIIa tail (positive control), GFP-tagged harmonin a, myc-tagged cadherin-23 cytodomain, myc-tagged protocadherin-15 cytodomain or myc-tagged sans (Supplementary Material, Fig. S5D). A binding was obtained with harmonin and sans, whereas no interaction was detected between βV-R29 and the cytodomain of either cadherin-23 or protocadherin-15 (Supplementary Material, Fig. S5D). These interactions were confirmed by direct *in vitro* binding experiments (Fig. 8C, and data not shown). We analysed also whether spectrin βV may interact with USH2 proteins, but failed to detect an interaction between the myc-tagged βV-R26 and GST-tagged fusion proteins of the usherin- and Vlgr1-cytodomains, or whirlin (Fig. 8D).

Sans, through its central domain, has been shown to bind directly to the first FERM domain of myosin VIIa, at nM affinity (68), indicating that the functioning of the two proteins is tightly linked *in vivo*. Indeed, it has been proposed that sans acts as an adaptor for the formation of the myosin VIIa/sans/harmonin tripartite complex (68), which explains why the

targeting of harmonin-b to the stereocilia tips depends on both myosin VIIa and sans (8,9,69). Myosin VIIa has been involved also in the transfer of other proteins, such as protocadherin-15 (USH1F), Usherin (USH2A), Vlgr1 (USH2C) and whrilin (USH2D) from the hair cell body to stereocilia (8,9,69,70). In the photoreceptor cells, spectrin βV-myosin VIIa and spectrin βV-sans complexes probably form and operate from the Golgi apparatus, moving upwards along the trafficking *route* towards the outer segment. Notably, of the dozens of myosin VIIa binding partners reported so far (5,71), spectrin βV is the first protein with the ability to bridge this motor protein to opsin containing vesicles (Fig. 3E). It is likely that a failure of the formation of myosin VIIa-spectrin βV-opsin complexes account for the abnormal accumulation of rhodopsin in the connecting cilium in myosin VIIa-deficient mice (32,35). Sans contribution to protein transport towards the outer segment is supported also by its interaction with myomegalin in the ellipsoid region (30). Interaction of the spectrin βV complex with harmonin may occur at the docking sites around the ciliary plasma membrane, serving as scaffolds between spectrin-tethered complexes and the cytoskeleton (Fig. 8B). It is noteworthy, however, that spectrin βV function in photoreceptor cells does not solely rely myosin VIIa and other USH1 proteins. Spectrin βV also interacts with the microtubule-based motors, which through their active role in transport, would explain why despite the absence of myosin VIIa, opsin transport was not completely abolished (32,35). Of note, spectrin βV is likely to bind other, yet uncovered, molecular complexes, especially via the spectrin repeats that form the long central region of the protein. Similar domains in other spectrins have, indeed, been involved in the stabilization of cytosolic and membrane proteins (36,37,49,50). Recently, it has been shown that myosin VIIa also directly interacts with the cyclic nucleotide gated channel α3, CNGA3, in the stereocilia of hair cells (72). CNGA3 is a subunit of the cone photoreceptor channel, an heterotetramer made up of two CNGA3 and CNGB3 subunits, which raises the question of whether myosin VIIa interacts also with the photoreceptor channels thereby contributing, cooperatively with spectrin βV and/or sans, to their transport towards the outer segment.

In summary, in addition to providing molecular explanations to the opsin transport delay in USH1B (myosin VIIa) mouse models, our findings extend the spectrin βV function to other phototransduction machinery and USH1 proteins. Finally, this study sheds light on the function of the spectrin β subunit, independently of its natural ligand, αII spectrin. We anticipate that similar, overlooked, situations that involve classical spectrin β subunits may be encountered in other cells, e.g. spectrin βIV without αII has been detected in axon initiation segments of neurons, surrounded by regions where spectrins αII/βII coexist (73,74). This points to the need to discriminate spectrin αII-dependent and -independent functions of spectrin multimers, especially regarding their role in protein sorting and targeting, in different cell types and varying wild-type and pathogenic cell contexts.

MATERIALS AND METHODS

Yeast two-hybrid screening

A human yeast two-hybrid (Y2H) retinal cDNA library was screened using the C-terminal MyTH4 and FERM domains (amino acids 1752–2215) of myosin VIIa as the bait (75). The positive Y2H clones were rescued, re-transformed into fresh L40 yeast cells and confirmed by growth on plates lacking histidine and β-galactosidase as described (75). The specificity of the positive clones was further tested by co-transformation with irrelevant baits; lamin C (accession number AAA36164) and merlin (accession number NP_001239179) used as negative controls.

Cloning and generation of DNA constructs

PCR-amplified fragments were first cloned into pCR2.1-TOPO (Invitrogen) and their sequences were checked prior to transfer to the appropriate vectors: i.e. pEGFP, pECFP and pEYFP (Clontech), pCMV-tag3B (Myc tag, Stratagene) and pcDNA3 (No tag, Flag or V5/His tag, Invitrogen) for *in vitro* translation and transfection experiments, and pXa3 (Biotin tag, Promega) or pGEX-// (GST tag, Amersham) for protein production.

The Y2H prey, referred to as βV-R29CT (amino acids 3355–3674), corresponds to the C-terminal region of spectrin βV (accession number AAF65317.1). Despite several attempts, we could not succeed to obtain full-length cDNAs encoding the entire spectrin βV, most probably because of the repetitive homologous sequences of the spectrin repeats in the large central domain (amino acids 256–3482; Fig. 1A, Supplementary Material, Fig. S1A). Two human cDNA clones containing spectrin βV full length were obtained from OriGene, but several errors and extended gaps were revealed by sequencing, essentially between the spectrin repeats 15 and 20. Nonetheless, we used these clones to engineer a chimeric mini-classical spectrin βV, hereafter referred to as βV-R7/21 (amino acids 2–1104 and 2473–3674), using a cDNA segment encoding amino acids 2–1104 and an additional segment encoding amino acids 2473 through the normal stop codon (Fig. 1F). This spectrin construct, which lacks the spectrin repeats 8 to 20, still retains the actin-binding domain, a central region with 17 spectrin repeats, and the C-terminal region containing the tetramerization site, and the C-terminal region containing the PH domain. The following spectrin βV fragments, βV-CH (amino acids 1–250), βV-R29 (amino acids 3317–3674), βV-R23 (amino acids 2684–3674), βV-R26 (amino acids 3002–3674) and βV-R29ΔPH (amino acids 3317–3530), and βV-PH (amino acids 3531–3643) were reconstituted using βV-R7/21 as a template. Recombinant pcDNA3 vectors encoding the extracellular and transmembrane domains of human E-cadherin fused to a ClaI–XbaI fragment encoding spectrin βV-R29 were used.

For spectrin βII (accession no. NP_008877.1), a fragment corresponding to βII-R13 (amino acids 1595–2363) was PCR-amplified from adult mouse brain cDNA.

As regards USH1 and USH2 proteins, different fusion proteins containing myosin VIIa full length (amino acids 1–2215, accession no. AAB03679.1), myosin VIIa tail (amino acids 847–2215); MyTH4/FERM fragment (amino acids 1752–2215), MyTH4 domain (amino acids 1731–1900), FERM domain (amino acids 1896–2215), harmonin a (amino acids 1–548, accession no. NP_076138), cadherin-23 cytodomain (amino acids 3086–3354, accession no. NP_075859), protocadherin-15 cytodomain (amino acids 1612–1943, accession no. Q99PJ1), sans (amino acids 1–461, accession no. NP_789817.1), usherin cytodomain (amino acids 5064–5193, accession no. Q2QI47),

Vlgr1 cytodomain (amino acids 6149–6298, accession no. Q8VHN7) or whirlin (amino acids 2–506, accession no. Q80VW5-3) were used. Other protein fragments: mouse myosin X tail (amino acids 811–2062, accession no. NP_062345.2), human myosin XVa C-terminal MyTH4-FERM (amino acids 2950–3511; accession no. NP_057323.3) and human ezrin (amino acids 1–586, accession no. NP_003370.2; gift from A. Alcover, Institut Pasteur, Paris, France). Mouse merlin (amino acids 1–580, accession no. P46662.2) and human full-length band 4.1G (accession no. O43491.1) were provided by J. Camonis (Institut Curie, Paris, France) and M Saito (University of Tohoku, Sendai, Japan), respectively.

Antibodies and reagents

The specificity of the purified anti-spectrin βV antibodies, directed against a human βV spectrin-fusion protein: amino acids 3443–3668, has been checked by immunocytofluorescence and immunoblot analysis (76). Rabbit anti-αII spectrin, and βIV spectrin antibodies were obtained from G. Nicolas (Paris, France), and M. Rasband (Boston, USA), respectively. The anti-myosin VIIa (antibody M1TN; 40), anti-cadherin-23 (antibody C1CDC, 77), and anti-sans (antibody S1SAM, 12), anti-harmonin (antibody H1N), anti-protocadherin-15 (antibody P1CD1-3), anti-usherin (antibody U2CD), anti-Vlgr1 (antibody V2CD), and anti-whirlin (antibody W2N) (24), anti-centrin (63) and anti-arrestin (66), have been described elsewhere.

The following additional antibodies and reagents were used: rabbit anti-GFP (Invitrogen), mouse anti-myc (sc-40, Santa Cruz), mouse anti-Flag2 tag (F3165, Sigma Aldrich), mouse anti-synaptophysin (Clone SVP-38, Sigma), mouse anti-β tubulin III (SDL.3D10, Sigma), mouse anti-βI spectrin (Novocostra) and mouse anti-spectrin βII (612562, BD). Rabbit anti-band 4.1G (C20), goat antibodies against βIII spectrin (sc-9660), anti-tranducins Gβ1 and Gβ3 were obtained from Santa Cruz Biotechnology. Rabbit anti-PDEγ was from R. Cote (University of New Hampshire, USA). Mouse anti-rhodopsin (Abcam), mouse anti-Lamp1 (611043) and mouse anti-GM130 (610822), mouse anti-dynamitin p50 (611003), mouse anti-Kif3a (611508), mouse anti-actin (612656) were from BD transduction laboratories. The other following antibodies, mouse anti-DIC74 (MAB1618, Millipore), mouse monoclonal anti-glutamylated tubulin (GT335) (ALX-804-885, Enzo Life Sciences), mouse anti-rhodopsin (MAB5316, Millipore) and goat polyclonal anti-cone opsin (sc-22117, Santa Cruz), were used.

Secondary antibodies (Invitrogen) were as follows: Alexa 488-goat anti-rabbit, Alexa-488-goat anti-mouse, Alexa-Fluor-488 donkey anti-goat, Cy3-anti-mouse and Cy3-anti-rabbit and DyLight 649 anti-mouse. TRITC-phalloidin (Sigma) and DAPI (1 μg/ml; Sigma) were used to label F-actin and nuclei, respectively.

Protein–protein interaction assays

For *in vitro* binding assays, GST-tagged and His-tagged fusion proteins were produced in BL21(DE3)-CodonPlus-RP *E. coli* cells and purified using glutathione Sepharose 4B (GE Healthcare). In several experiments radiolabeled untagged proteins were translated with the T7/T3-coupled transcription–translation system (Promega) according to the manufacturer's instructions. Equal amounts of either fusion proteins or GST alone were used as described (76). Briefly, to test the spectrin βV-myosin VIIa direct interaction, a bacterial lysate containing GST alone or GST-tagged βV-R29 was incubated with pre-equilibrated glutathione-Sepharose beads for 90 min at 4°C. The beads were washed three times with binding buffer (5% glycerol, 5 mM $MgCl_2$ and 0.1% Triton X-100 in phosphate-buffered saline) supplemented with a protease inhibitor cocktail (Roche), and then incubated with the *in vitro* translated ^{35}S-labeled myosin VIIa (amino acids 1–2215) for 3 h at 4°C on a rotating wheel. The beads were then washed four times with the binding buffer supplemented with 150 mM NaCl. Bound proteins were resuspended in 30 μl 2× concentrated SDS sample buffer, and analysed on a 4–12% SDS–polyacrylamide gel. The gel was stained with Coomassie blue, dried and processed for autoradiography. For GST pull down assays, beads were incubated overnight with soluble protein extracts obtained from transfected HEK293 cells or adult rat retinas. Beads were then washed three times with binding buffer supplemented with 150 mM NaCl. Bound proteins were resuspended in 30 μl 2× concentrated SDS sample buffer, and analysed by western blot. Horseradish peroxidase (HRP)-conjugated goat anti-rabbit or anti-mouse antibodies (Jackson ImmunoResearch) and the ECL chemiluminescence system (Pierce) were used for detection.

Immunofluorescence and electron microscopy analyses

Eyes and inner ears from monkeys, humans and mice were used. Eyes were collected from adult cynomolgus monkeys (Macaca fascicularis) housed at the MIRcen platform (CEA/INSERM, Fontenay-aux-Roses, France), when killed as controls in other unrelated experiments. Human retinas were obtained several hours after death from the Minnesota Lions Eye Bank (Minneapolis, MN, USA). All the experiments on animals were carried out according to protocols approved by the Animal Use Committees of INSERM, CEA (for monkeys), Institut Pasteur and the ARVO Statement for the Use of Animals in Ophthalmic and Vision Research.

Monkey, human or mouse eyecups were fixed in 4% paraformaldehyde in phosphate buffer, pH 7.4, at 4°C for about 1–2 h and infused sequentially for 12 h with 15 and 30% sucrose, then embedded in OCT medium, frozen in dry ice and kept at −80°C until use. Immunohistochemistry on retinal sections was carried out as previously described (24). The sections were labelled overnight with the primary antibody diluted in PBS containing 0.1% Triton X-100 and 5% normal goat serum. Sections were rinsed in PBS, labelled for 1 h with appropriate secondary antibodies, and counterstained with DAPI nuclear stain and/or TRITC-phalloidin. Images were collected using a Zeiss LSM700 Meta confocal microscope (Carl Zeiss MicroImaging, Inc.) equipped with a plan Apo 63x NA 1.4 oil immersion objective lens.

For immunoelectron microscopy, we adopted post-embedding and pre-embedding protocols as previously described (35,61,78), respectively. Adult C57BL/6J mice were maintained under a 12 h light–dark cycle, with food and water *ad libitum*. After sacrifice of the animals in CO_2 and decapitation, subsequently entire eyeballs and appropriate tissues were

dissected and processed for post-embedding labelling. Following guidelines to the Declaration of Helsinki, a human eye was obtained from the Dept. of Ophthalmology, Mainz, Germany and used for the pre-embedding procedure. Ultrathin sections were analysed in a transmission electron microscope (Tecnai 12 BioTwin; FEI, Eindhoven, The Netherlands). Images were obtained with a charge-coupled device camera (SIS Megaview3; Surface Imaging Systems) acquired by analySIS (Soft Imaging System) and processed with Photoshop CS6.

Immunoprecipitation experiments

Lysates derived from human embryonic kidney HEK293 cells or from mouse or rat tissues were used. Transient transfections were performed at 90–95% confluency according to the manufacturer's recommendation, using Lipofectamine 2000 reagent (Invitrogen) as described (76). In some experiments, μMACS anti-GFP coated beads were used to coimmunoprecipitate GFP-tagged proteins, according to supplier's recommendations (Milteny Biotec SAS, France). The HEK293 cell protein extracts or adult rat retina extracts were prepared by using 500 μl of immunoprecipitation buffer (150 mM NaCl, 50 mM Tris–HCl, pH 7.5, 500 μM EDTA, 100 μM EGTA, 0.1% SDS, 1% Triton X-100 and 1% sodium deoxycholate), complemented with an EDTA-free cocktail of protease inhibitors (Roche). The soluble fraction was incubated for 6 h either with the anti-spectrin βV, the pre-immune serum or immunoprecipitation buffer alone, then with 50 μl of pre-equilibrated protein G beads (Pierce) at 4°C overnight. After three washes with immunoprecipitation buffer, bound complexes were electrotransferred to nitrocellulose sheets and probed with appropriate antibodies. HRP-conjugated goat anti–rabbit antibodies (GE Healthcare) and the ECL chemiluminescence system (Pierce) were used for detection.

Lamp1 immunofluorescence analysis

HeLa cells were cultivated in Invitrogen D-MEM with GLUTAMAX I and sodium pyruvate medium supplemented with 10% fetal bovine serum, 50 U/ml penicillin and 50 μg/ml streptomycin (Invitrogen). HeLa cells were transfected with Lipofectamine 2000 reagent (Invitrogen) according to the instructions of the manufacturer: with spectrin βV-R26, spectrin βV-R7/21 or spectrin βII-R13, fixed in 4% PFA and labelled. Stained cells on cover slips were mounted with FluorSaveTM reagent (Calbiochem, France) for imaging using an LSM 700 confocal laser scanning microscope (Carl Zeiss; 63x oil-immersion lens, 1.40 NA, LSM 700 software). For fluorescence quantification, the ImageJ software version 1.45f (NIH) was used to measure Lamp1 integrated fluorescence in the cytoplasm of transfected and not transfected cells. To minimize the variation in fluorescence intensities from image to image, we compared images acquired during the same session under identical settings and immunostained in the same experiment with the same pool of antibodies. For each cell, Lamp1 fluorescence was normalized dividing it by the nucleus area of the cell. Statistical analysis was performed using GraphPad Prism software. Data were analysed by the Mann–Whiney test.

Fluorescence resonance energy transfer microscopy (FRET) experiments

To visualize spectrin βV self-association in a cellular context, we used two expression vectors encoding spectrin fusion proteins with either CFP or YFP fluorophores tethered to their amino-terminal region. CFP-tagged βV-R23 (amino acids 2684–3674) and YFP-tagged βV-R29 (amino acids 3317–3674) were used as donor and acceptor, respectively. After transient (co)transfection of HeLa cells, intracellular distribution of YFP-tagged βV-R29 or CFP-tagged βV-R23 fluorescence was imaged by confocal laser scanning microscopy. All experiments were performed between 24 and 48 h post-transfection. The excitation wavelength was 445 nm. The cyan (CFP) and yellow (YFP) fluorescence (lifetime) of the fusion proteins is monitored by use of a fluorescent protein-specific emission filters, BP455-495 for CFP, and BP 495–555 for YFP. A Lambert Instruments (The Netherlands) Lifa-X coupled to a Zeiss Axiovert 200M via a Yokogawa CSU22 Spinning Disc head was used to determine the fluorescence lifetimes of the fluorescent proteins. The system was calibrated using 10 μM fluorescein in ethanol (standard lifetime of 4 ns). The 445 nm laser and intensifier of the CCD were modulated at 40 MHz, the exposure time set to 300 ms and 12 images at different pseudo-random phase delays were acquired. The data were analysed using the commercial software. Measurements were made from multiple individual cells in each culture plate. Values are presented as mean ± standard error of the mean (SEM). The double asterisk denotes statistically significant difference in Student's *t*-test, with $P < 0.01$.

SUPPLEMENTARY MATERIAL

Supplementary Material is available at *HMG* online.

ACKNOWLEDGEMENTS

We thank G. Nicolas, B. Vannier, A. Alcover, R. Cote, Y. Araki, M. Rasband and M. Saito for providing us with reagents, P. Kussel for her assistance and J-P. Hardelin for his critical comments on the manuscript.

Conflict of Interest statement. None declared.

FUNDING

This work was supported by the Agence Nationale de la recherche (ANR-07-MRARE-009-01), European Union Seventh Framework Programme, under grant agreement HEALTH-F2-2010-242013 (TREATRUSH), European Community's Seventh Framework Programme FP7/2009 under grant agreement number 241955 (SYSCILIA), LHW-Stiftung, Fondation Raymonde & Guy Strittmatter, Fighting Blindness, FAUN Stiftung (Suchert Foundation), Conny Maeva Charitable Foundation, Fondation Orange, ERC grant 294570-hair bundle, the French State program 'Investissements d'Avenir' managed by the Agence Nationale de la Recherche (ANR-10-LABX-65), 'the Foundation Fighting Blindness Paris Center Grant' and the Fondation Voir et Entendre. S.P. benefited from two fellowships from MNERT (UPMC-CdV) and 'Fondation Retina-France'.

REFERENCES

1. El-Amraoui, A. and Petit, C. (2005) Usher I syndrome: unravelling the mechanisms that underlie the cohesion of the growing hair bundle in inner ear sensory cells. *J. Cell Sci.*, **118**, 4593–4603.
2. Petit, C. and Richardson, G.P. (2009) Linking deafness genes to hair-bundle development and function. *Nat. Neurosci.*, **12**, 703–710.
3. Richardson, G.P., de Monvel, J.B. and Petit, C. (2011) How the genetics of deafness illuminates auditory physiology. *Annu. Rev. Physiol.*, **73**, 311–334.
4. Friedman, T.B., Schultz, J.M., Ahmed, Z.M., Tsilou, E.T. and Brewer, C.C. (2011) Usher syndrome: hearing loss with vision loss. *Adv. Otorhinolaryngol.*, **70**, 56–65.
5. Pan, L. and Zhang, M. (2012) Structures of usher syndrome 1 proteins and their complexes. *Physiology (Bethesda)*, **27**, 25–42.
6. Bonnet, C. and El-Amraoui, A. (2012) Usher syndrome (sensorineural deafness and retinitis pigmentosa): pathogenesis, molecular diagnosis and therapeutic approaches. *Curr. Opin. Neurol.*, **25**, 42–49.
7. Riazuddin, S., Belyantseva, I.A., Giese, A.P., Lee, K., Indzhykulian, A.A., Nandamuri, S.P., Yousaf, R., Sinha, G.P., Lee, S., Terrell, D. *et al.* (2012) Alterations of the CIB2 calcium- and integrin-binding protein cause Usher syndrome type 1J and nonsyndromic deafness DFNB48. *Nat. Genet.*, **44**, 1265–1271.
8. Lefèvre, G., Michel, V., Weil, D., Lepelletier, L., Bizard, E., Wolfrum, U., Hardelin, J.P. and Petit, C. (2008) A core cochlear phenotype in USH1 mouse mutants implicates fibrous links of the hair bundle in its cohesion, orientation and differential growth. *Development*, **135**, 1427–1437.
9. Boëda, B., El-Amraoui, A., Bahloul, A., Goodyear, R., Daviet, L., Blanchard, S., Perfettini, I., Fath, K.R., Shorte, S., Reiners, J. *et al.* (2002) Myosin VIIa, harmonin and cadherin 23, three Usher I gene products that cooperate to shape the sensory hair cell bundle. *EMBO J.*, **21**, 6689–6699.
10. Kazmierczak, P., Sakaguchi, H., Tokita, J., Wilson-Kubalek, E.M., Milligan, R.A., Muller, U. and Kachar, B. (2007) Cadherin 23 and protocadherin 15 interact to form tip-link filaments in sensory hair cells. *Nature*, **449**, 87–91.
11. Grati, M. and Kachar, B. (2011) Myosin VIIa and sans localization at stereocilia upper tip-link density implicates these Usher syndrome proteins in mechanotransduction. *Proc. Natl Acad. Sci. USA*, **108**, 11476–11481.
12. Caberlotto, E., Michel, V., Foucher, I., Bahloul, A., Goodyear, R.J., Pepermans, E., Michalski, N., Perfettini, I., Alegria-Prevot, O., Chardenoux, S. *et al.* (2011) Usher type 1G protein sans is a critical component of the tip-link complex, a structure controlling actin polymerization in stereocilia. *Proc. Natl Acad. Sci. USA*, **108**, 5825–5830.
13. Flores-Guevara, R., Renault, F., Loundon, N., Marlin, S., Pelosse, B., Momtchilova, M., Auzoux-Cheve, M., Vermersch, A.I. and Richard, P. (2009) Usher syndrome type 1: early detection of electroretinographic changes. *Eur. J. Paediatr. Neurol.*, **13**, 505–507.
14. Jacobson, S.G., Cideciyan, A.V., Gibbs, D., Sumaroka, A., Roman, A.J., Aleman, T.S., Schwartz, S.B., Olivares, M.B., Russell, R.C., Steinberg, J.D. *et al.* (2011) Retinal disease course in usher syndrome 1B due to MYO7A mutations. *Invest. Ophthalmol. Vis. Sci.*, **52**, 7924–7936.
15. Malm, E., Ponjavic, V., Moller, C., Kimberling, W.J. and Andreasson, S. (2011) Phenotypes in defined genotypes including siblings with Usher syndrome. *Ophthalmic Genet.*, **32**, 65–74.
16. Malm, E., Ponjavic, V., Moller, C., Kimberling, W.J., Stone, E.S. and Andreasson, S. (2011) Alteration of rod and cone function in children with Usher syndrome. *Eur. J. Ophthalmol.*, **21**, 30–38.
17. Libby, R.T., Kitamoto, J., Holme, R.H., Williams, D.S. and Steel, K.P. (2003) Cdh23 mutations in the mouse are associated with retinal dysfunction but not retinal degeneration. *Exp. Eye Res.*, **77**, 731–739.
18. Libby, R.T. and Steel, K.P. (2001) Electroretinographic anomalies in mice with mutations in Myo7a, the gene involved in human Usher syndrome type 1B. *Invest. Ophthalmol. Vis. Sci.*, **42**, 770–778.
19. Ball, S.L., Bardenstein, D. and Alagramam, K.N. (2003) Assessment of retinal structure and function in Ames waltzer mice. *Invest. Ophthalmol. Vis. Sci.*, **44**, 3986–3992.
20. Johnson, K.R., Gagnon, L.H., Webb, L.S., Peters, L.L., Hawes, N.L., Chang, B. and Zheng, Q.Y. (2003) Mouse models of USH1C and DFNB18: phenotypic and molecular analyses of two new spontaneous mutations of the Ush1c gene. *Hum. Mol. Genet.*, **12**, 3075–3086.
21. Haywood-Watson, R.J. 2nd, Ahmed, Z.M., Kjellstrom, S., Bush, R.A., Takada, Y., Hampton, L.L., Battey, J.F., Sieving, P.A. and Friedman, T.B. (2006) Ames Waltzer deaf mice have reduced electroretinogram amplitudes and complex alternative splicing of Pcdh15 transcripts. *Invest. Ophthalmol. Vis. Sci.*, **47**, 3074–3084.
22. Williams, D.S. (2008) Usher syndrome: animal models, retinal function of Usher proteins, and prospects for gene therapy. *Vision Res.*, **48**, 433–441.
23. Williams, D.S., Aleman, T.S., Lillo, C., Lopes, V.S., Hughes, L.C., Stone, E.M. and Jacobson, S.G. (2009) Harmonin in the murine retina and the retinal phenotypes of Ush1c-mutant mice and human USH1C. *Invest. Ophthalmol. Vis. Sci.*, **50**, 3881–3889.
24. Sahly, I., Dufour, E., Schietroma, C., Michel, V., Bahloul, A., Perfettini, I., Pepermans, E., Estivalet, A., Carette, D., Aghaie, A. *et al.* (2012) Localization of Usher 1 proteins to the photoreceptor calyceal processes, which are absent from mice. *J. Cell Biol.*, **199**, 381–399.
25. Reiners, J., Reidel, B., El-Amraoui, A., Boeda, B., Huber, I., Petit, C. and Wolfrum, U. (2003) Differential distribution of harmonin isoforms and their possible role in Usher-1 protein complexes in mammalian photoreceptor cells. *Invest. Ophthalmol. Vis. Sci.*, **44**, 5006–5015.
26. El-Amraoui, A., Schonn, J.-S., Küssel-Andermann, P., Blanchard, S., Desnos, C., Henry, J.-P., Wolfrum, U., Darchen, F. and Petit, C. (2002) MyRIP, a novel Rab effector, enables myosin VIIa recruitment to retinal melanosomes. *EMBO Rep.*, **3**, 463–470.
27. Gibbs, D., Kitamoto, J. and Williams, D.S. (2003) Abnormal phagocytosis by retinal pigmented epithelium that lacks myosin VIIa, the Usher syndrome 1B protein. *Proc. Natl Acad. Sci. USA*, **100**, 6481–6486.
28. Gibbs, D., Azarian, S.M., Lillo, C., Kitamoto, J., Klomp, A.E., Steel, K.P., Libby, R.T. and Williams, D.S. (2004) Role of myosin VIIa and Rab27a in the motility and localization of RPE melanosomes. *J. Cell Sci.*, **117**, 6473–6483.
29. Maerker, T., van Wijk, E., Overlack, N., Kersten, F.F., McGee, J., Goldmann, T., Sehn, E., Roepman, R., Walsh, E.J., Kremer, H. *et al.* (2008) A novel Usher protein network at the periciliary reloading point between molecular transport machineries in vertebrate photoreceptor cells. *Hum. Mol. Genet.*, **17**, 71–86.
30. Overlack, N., Kilic, D., Bauss, K., Marker, T., Kremer, H., van Wijk, E. and Wolfrum, U. (2011) Direct interaction of the Usher syndrome 1G protein SANS and myomegalin in the retina. *Biochim. Biophys. Acta*, **1813**, 1883–1892.
31. Liu, X., Ondek, B. and Williams, D.S. (1998) Mutant myosin VIIa causes defective melanosome distribution in the RPE of shaker-1 mice. *Nat. Genet.*, **19**, 117–118.
32. Liu, X., Udovichenko, I.P., Brown, S.D., Steel, K.P. and Williams, D.S. (1999) Myosin VIIa participates in opsin transport through the photoreceptor cilium. *J. Neurosci.*, **19**, 6267–6274.
33. Marszalek, J.R., Liu, X., Roberts, E.A., Chui, D., Marth, J.D., Williams, D.S. and Goldstein, L.S. (2000) Genetic evidence for selective transport of opsin and arrestin by kinesin-II in mammalian photoreceptors. *Cell*, **102**, 175–187.
34. Jimeno, D., Feiner, L., Lillo, C., Teofilo, K., Goldstein, L.S., Pierce, E.A. and Williams, D.S. (2006) Analysis of kinesin-2 function in photoreceptor cells using synchronous Cre-loxP knockout of Kif3a with RHO-Cre. *Invest. Ophthalmol. Vis. Sci.*, **47**, 5039–5046.
35. Wolfrum, U. and Schmitt, A. (2000) Rhodopsin transport in the membrane of the connecting cilium of mammalian photoreceptor cells. *Cell Motil. Cytoskeleton*, **46**, 95–107.
36. De Matteis, M.A. and Morrow, J.S. (2000) Spectrin tethers and mesh in the biosynthetic pathway. *J. Cell Sci.*, **113**, 2331–2343.
37. Bennett, V. and Healy, J. (2009) Membrane domains based on ankyrin and spectrin associated with cell-cell interactions. *Cold Spring Harb. Perspect. Biol.*, **1**, a003012.
38. Stabach, P.R. and Morrow, J.S. (2000) Identification and characterization of beta V spectrin, a mammalian ortholog of Drosophila beta H spectrin. *J. Biol. Chem.*, **275**, 21385–21395.
39. Etournay, R., El-Amraoui, A., Bahloul, A., Blanchard, S., Roux, I., Pezeron, G., Michalski, N., Daviet, L., Hardelin, J.P., Legrain, P. *et al.* (2005) PHR1, an integral membrane protein of the inner ear sensory cells, directly interacts with myosin 1c and myosin VIIa. *J. Cell Sci.*, **118**, 2891–2899.
40. El-Amraoui, A., Sahly, I., Picaud, S., Sahel, J., Abitbol, M. and Petit, C. (1996) Human Usher IB/mouse *shaker-1*; the retinal phenotype discrepancy explained by the presence/absence of myosin VIIA in the photoreceptor cells. *Hum. Mol. Genet.*, **5**, 1171–1178.
41. Liu, X., Vansant, G., Udovichenko, I.P., Wolfrum, U. and Williams, D.S. (1997) Myosin VIIa, the product of the Usher 1B syndrome gene, is concentrated in the connecting cilia of photoreceptor cells. *Cell Motil. Cytoskeleton*, **37**, 240–252.

42. Wolfrum, U., Liu, X., Schmitt, A., Udovichenko, I.P. and Williams, D.S. (1998) Myosin VIIa as a common component of cilia and microvilli. *Cell Motil. Cytoskeleton*, **40**, 261–271.
43. Young, R.W. (1967) The renewal of photoreceptor cell outer segments. *J. Cell Biol.*, **33**, 61–72.
44. Papermaster, D.S. (2002) The birth and death of photoreceptors: the Friedenwald Lecture. *Invest. Ophthalmol. Vis. Sci.*, **43**, 1300–1309.
45. Mayhew, T.M. and Astle, D. (1997) Photoreceptor number and outer segment disk membrane surface area in the retina of the rat: stereological data for whole organ and average photoreceptor cell. *J. Neurocytol.*, **26**, 53–61.
46. Insinna, C. and Besharse, J.C. (2008) Intraflagellar transport and the sensory outer segment of vertebrate photoreceptors. *Dev. Dyn.*, **237**, 1982–1992.
47. Yau, K.W. and Hardie, R.C. (2009) Phototransduction motifs and variations. *Cell*, **139**, 246–264.
48. Besharse, J.C. and Wetzel, M.G. (1995) Immunocytochemical localization of opsin in rod photoreceptors during periods of rapid disc assembly. *J. Neurocytol.*, **24**, 371–388.
49. Baines, A.J. (2009) Evolution of spectrin function in cytoskeletal and membrane networks. *Biochem. Soc. Trans.*, **37**, 796–803.
50. Baines, A.J. (2010) The spectrin-ankyrin-4.1-adducin membrane skeleton: adapting eukaryotic cells to the demands of animal life. *Protoplasma*, **244**, 99–131.
51. Kizhatil, K., Baker, S.A., Arshavsky, V.Y. and Bennett, V. (2009) Ankyrin-G promotes cyclic nucleotide-gated channel transport to rod photoreceptor sensory cilia. *Science*, **323**, 1614–1617.
52. Kizhatil, K., Sandhu, N.K., Peachey, N.S. and Bennett, V. (2009) Ankyrin-B is required for coordinated expression of beta-2-spectrin, the Na/K-ATPase and the Na/Ca exchanger in the inner segment of rod photoreceptors. *Exp. Eye Res.*, **88**, 57–64.
53. Lee, J.K., Coyne, R.S., Dubreuil, R.R., Goldstein, L.S. and Branton, D. (1993) Cell shape and interaction defects in alpha-spectrin mutants of Drosophila melanogaster. *J. Cell Biol.*, **123**, 1797–1809.
54. Clarkson, Y.L., Gillespie, T., Perkins, E.M., Lyndon, A.R. and Jackson, M. (2010) Beta-III spectrin mutation L253P associated with spinocerebellar ataxia type 5 interferes with binding to Arp1 and protein trafficking from the Golgi. *Hum. Mol. Genet.*, **19**, 3634–3641.
55. Williams, J.A., MacIver, B., Klipfell, E.A. and Thomas, G.H. (2004) The C-terminal domain of Drosophila (beta) heavy-spectrin exhibits autonomous membrane association and modulates membrane area. *J. Cell Sci.*, **117**, 771–782.
56. Phillips, M.D. and Thomas, G.H. (2006) Brush border spectrin is required for early endosome recycling in Drosophila. *J. Cell Sci.*, **119**, 1361–1370.
57. Rosenbaum, J.L. and Witman, G.B. (2002) Intraflagellar transport. *Nat. Rev. Mol. Cell Biol.*, **3**, 813–825.
58. Liu, Q., Zhang, Q. and Pierce, E.A. (2010) Photoreceptor sensory cilia and inherited retinal degeneration. *Adv. Exp. Med. Biol.*, **664**, 223–232.
59. Tai, A.W., Chuang, J.Z., Bode, C., Wolfrum, U. and Sung, C.H. (1999) Rhodopsin's carboxy-terminal cytoplasmic tail acts as a membrane receptor for cytoplasmic dynein by binding to the dynein light chain Tctex-1. *Cell*, **97**, 877–887.
60. Roepman, R. and Wolfrum, U. (2007) Protein networks and complexes in photoreceptor cilia. *Subcell. Biochem.*, **43**, 209–235.
61. Sedmak, T. and Wolfrum, U. (2010) Intraflagellar transport molecules in ciliary and nonciliary cells of the retina. *J. Cell Biol.*, **189**, 171–186.
62. Liu, Q., Tan, G., Levenkova, N., Li, T., Pugh, E.N. Jr, Rux, J.J., Speicher, D.W. and Pierce, E.A. (2007) The proteome of the mouse photoreceptor sensory cilium complex. *Mol. Cell Proteomics*, **6**, 1299–1317.
63. Trojan, P., Krauss, N., Choe, H.W., Giessl, A., Pulvermuller, A. and Wolfrum, U. (2008) Centrins in retinal photoreceptor cells: regulators in the connecting cilium. *Prog. Retin. Eye Res.*, **27**, 237–259.
64. Swaroop, A., Kim, D. and Forrest, D. (2010) Transcriptional regulation of photoreceptor development and homeostasis in the mammalian retina. *Nat. Rev. Neurosci.*, **11**, 563–576.
65. Sung, C.H. and Chuang, J.Z. (2010) The cell biology of vision. *J. Cell Biol.*, **190**, 953–963.
66. Reidel, B., Goldmann, T., Giessl, A. and Wolfrum, U. (2008) The translocation of signaling molecules in dark adapting mammalian rod photoreceptor cells is dependent on the cytoskeleton. *Cell Motil. Cytoskeleton*, **65**, 785–800.
67. Peng, Y.W., Zallocchi, M., Wang, W.M., Delimont, D. and Cosgrove, D. (2011) Moderate light-induced degeneration of rod photoreceptors with delayed transducin translocation in shaker1 mice. *Invest. Ophthalmol. Vis. Sci.*, **52**, 6421–6427.
68. Wu, L., Pan, L., Wei, Z. and Zhang, M. (2011) Structure of MyTH4-FERM domains in myosin VIIa tail bound to cargo. *Science*, **331**, 757–760.
69. Michalski, N., Michel, V., Bahloul, A., Lefevre, G., Barral, J., Yagi, H., Chardenoux, S., Weil, D., Martin, P., Hardelin, J.P. *et al.* (2007) Molecular characterization of the ankle-link complex in cochlear hair cells and its role in the hair bundle functioning. *J. Neurosci.*, **27**, 6478–6488.
70. Senften, M., Schwander, M., Kazmierczak, P., Lillo, C., Shin, J.B., Hasson, T., Geleoc, G.S., Gillespie, P.G., Williams, D., Holt, J.R. *et al.* (2006) Physical and functional interaction between protocadherin 15 and myosin VIIa in mechanosensory hair cells. *J. Neurosci.*, **26**, 2060–2071.
71. El-Amraoui, A., Bahloul, A. and Petit, C. (2008) Myosin VII. *Myosins, A Superfamily of Molecular Motors*, Springer, Dordrecht, Netherlands, Vol. 7, pp. 353–373.
72. Selvakumar, D., Drescher, M.J. and Drescher, D.G. (2013) CNGA3 interacts with Stereocilia tip-link protein cadherin 23 +68 or alternatively with myosin VIIa, two proteins required for hair cell mechanotransduction. *J. Biol. Chem.*, **288**, 7215–7229.
73. Lacas-Gervais, S., Guo, J., Strenzke, N., Scarfone, E., Kolpe, M., Jahkel, M., De Camilli, P., Moser, T., Rasband, M.N. and Solimena, M. (2004) BetaIVSigma1 spectrin stabilizes the nodes of Ranvier and axon initial segments. *J. Cell Biol.*, **166**, 983–990.
74. Ogawa, Y., Schafer, D.P., Horresh, I., Bar, V., Hales, K., Yang, Y., Susuki, K., Peles, E., Stankewich, M.C. and Rasband, M.N. (2006) Spectrins and ankyrinB constitute a specialized paranodal cytoskeleton. *J. Neurosci.*, **26**, 5230–5239.
75. Kussel-Andermann, P., El-Amraoui, A., Safieddine, S., Hardelin, J.P., Nouaille, S., Camonis, J. and Petit, C. (2000) Unconventional myosin VIIA is a novel A-kinase-anchoring protein. *J. Biol. Chem.*, **275**, 29654–29659.
76. Legendre, K., Safieddine, S., Kussel-Andermann, P., Petit, C. and El-Amraoui, A. (2008) αII/βV spectrin bridges the plasma membrane and cortical lattice in the lateral wall of auditory outer hair cells. *J. Cell Sci.*, **121**, 3347–3356.
77. Bahloul, A., Michel, V., Hardelin, J.P., Nouaille, S., Hoos, S., Houdusse, A., England, P. and Petit, C. (2010) Cadherin-23, myosin VIIa and harmonin, encoded by Usher syndrome type I genes, form a ternary complex and interact with membrane phospholipids. *Hum. Mol. Genet.*, **19**, 3557–3565.
78. Sedmak, T., Sehn, E. and Wolfrum, U. (2009) Immunoelectron microscopy of vesicle transport to the primary cilium of photoreceptor cells. *Methods Cell Biol.*, **94**, 259–272.